Technion Research &
Development Foundation Ltd.

Israel Institute of Metals

Prediction of Fatigue Crack Growth under Constant Amplitude and Random Loading Using Specimens with Multiple Cracks.

Technion Research No. 524727

Supported by U.S.A.F.

October 1, 1993 - September 30, 1994

S. Ustilovsky

R. Arone

J. Oshrat

E. Sterin

G. Nesviszsky

Technion - Haifa 1994

REPORT DOCUMENTATION PAGE

Form Approved
OMB No. 0704-0188

1. AGENCY USE ONLY (Leave blank)	2. REPORT DATE	3. REPORT TYPE AND DATES COVERED
	December 1994	Final report (1 Oct 93-30 Sept 94)

4. TITLE AND SUBTITLE
Prediction of Fatigue Crack Growth under CA and Random Loading Using Specimens with Multiple Cracks

5. FUNDING NUMBERS
Grant No.
F49620-93-1-0579

6. AUTHOR(S)
Sh. Ustilovsky, R. Arone, J. Oshrat, E. Sterin, G. Nesviszsky

7. PERFORMING ORGANIZATION NAME(S) AND ADDRESS(ES)
Israel Institute of Metals, Technion R&D Foundation Ltd.
Technion City, Haifa 32000, Israel

8. PERFORMING ORGANIZATION REPORT NUMBER
524727.

9. SPONSORING/MONITORING AGENCY NAME(S) AND ADDRESS(ES)
EOARD/LDS
223/231 Old Marylebone Road, London, NW1 5TH, UK

10. SPONSORING/MONITORING AGENCY REPORT NUMBER
TR-95-06

11. SUPPLEMENTARY NOTES

12a. DISTRIBUTION/AVAILABILITY STATEMENT
Unclassified - Unlimited

12b. DISTRIBUTION CODE

13. ABSTRACT (Maximum 200 words)

Fatigue crack growth under stationary Gaussian random loading is considered. A specially developed computerised testing system and software are used for generation of the random loading and investigation of crack growth. The sliding summation numerical method was used for generation of a random loading history characterized by a given autocorrelation function. As far as the loading history of a sufficient length is generated a sequence of maxima and minima is extracted and arranged with the predetermined frequency. The next operation is elimination of the small amplitude cycles in accordance with the predetermined threshold value and determination of the minima and maxima two-dimensional distribution of the edited process. A specially built transition matrix derived from this distribution was used for the real-time generation of the random loading during the test. Experimental investigation of the developed random loading generation procedure and crack growth process was performed using aluminium alloy multicrack panel type specimens providing possibility of observation of an array of simultaneously growing cracks. Dependence of fatigue crack life time on random loading parameters as well as stochastic characteristics of crack growth were studied.

14. SUBJECT TERMS	15. NUMBER OF PAGES
Fatigue, Random Loading, Crack Growth, Overloads	71
	16. PRICE CODE

17. SECURITY CLASSIFICATION OF REPORT	18. SECURITY CLASSIFICATION OF THIS PAGE	19. SECURITY CLASSIFICATION OF ABSTRACT	20. LIMITATION OF ABSTRACT
Unclassified	Unclassified	Unclassified	

TR-95-06

This report has been reviewed and is releasable to the National Technical Information Service (NTIS). At NTIS it will be releasable to the general public, including foreign nations.

This technical report has been reviewed and is approved for publication.

DANIEL J. STECH, Maj, USAF
Chief, Aerospace Structures & Structural Materials

DONALD R. ERBSCHLOE, Lt Col, USAF
Chief, International Programs

TR-95-06

Technion Research &
Development Foundation Ltd.

Israel Institute of Metals

Prediction of Fatigue Crack Growth under Constant Amplitude and Random Loading Using Specimens with Multiple Cracks.

Technion Research No. 524727

Supported by U.S.A.F.

October 1, 1993 - September 30, 1994

S. Ustilovsky

R. Arone

J. Oshrat

E. Sterin

G. Nesviszky

Technion - Haifa 1994

CONTENTS

1. Introduction

The work presented in this report is devoted to the study of the stochastic behaviour of arrays of fatigue cracks simultaneously growing in aircraft quality aluminium alloy sheets. This work was sponsored by the European Office of Aerospace Research and Development of the U.S. Air Force. The objectives of the work are investigation of probabilistic parameters characterizing fatigue crack growth under different types of loading history: 1) constant amplitude (CA) loading, 2) CA-loading with superimposed overloads (CAO), 3) random loading (RL), and 4) random loading with superimposed overloads (RLO).

The initial research program envisages two year work, and the results of the first year work are presented in this report. Performed investigation is based on an application of so-called multi-crack specimens [1,2] i.e., the panel-type sheet specimen comprising arrays of parallel edge cracks on both edges of the panel. Detailed description of the specimen is given below. One of the advantages of the application of the multicrack specimen is identity of loading history for all the cracks in an array, which is quite difficult to ensure in single crack specimens due to unavoidable deviations in loading histories under separate tests.

Application of the multicrack specimens permits investigation of crack interaction in the course of fatigue process. As far as the distance between the cracks is sufficiently large the interaction between the cracks can be neglected. On the contrary in the case of small intercrack spacing the interaction is significant; thus varying the intercrack spacing different degrees of crack interaction can be studied. The notion of sufficiently long intercrack distance depends on the crack length, the longer the cracks the greater should be the distance sufficient to ensure noninteraction.

The work presented in this report deals with the experimental study of the fatigue growth of relatively short (i.e., noninteracting) cracks in an aluminium alloy

7075-T6 under CA, CAO, RL and RLO loadings. The work comprises the following stages:

- Selection and ordering of experimental material,
- Choice of specimen configuration and location of prenotches (necessary to initiate crack growth) on the both edges of the specimen,
- Machining of the specimens and this preparation for crack growth monitoring: attachment of crack propagation and strain gauges, wiring and running-in of measuring circuits,
- Development of a procedure for appropriate specimen installation within the Instron machine frame, ensuring axiality of applied loads,
- Running-in of the whole system intended for monitoring the stresses and crack lengths during the loading process, as well as for control of the testing machine,
- Development of a software for generation of various types of loading histories, including RL and RLO,
- Investigation of crack growth under CA-loading,
- Determination of crack growth delay times caused by single overloads superimposed on CA-loading,
- Investigation of crack growth under series of RL loading histories characterised by different parameters of the process (average, standard deviation),
- Investigation of crack growth under RLO,
- Analysis of obtained experimental data.

Future work will comprise

- Investigation of crack interaction and its influence on crack growth under different loading histories,
- Determination of statistical parameters characterising fatigue crack growth,
- Development of a mathematical model describing fatigue crack growth in a random medium and under different random loading histories.

2. Specimens, Testing Equipment and Devices

2.1 Material

The 7075-T6 aluminium alloy, widely used in the aircraft industry was selected as an experimental material. A number of 2-mm-thickness sheets with the width 1200mm and length 3600mm were purchased. Transverse tensile specimens (corresponding to the specimen of 12.5mm width) were tested in accordance with the ASTM E8-93 standard [3] to determine mechanical properties of the purchased material.

Test results are shown in Table 1, as well as the typical properties according to the SAE J454-91 standard [4].

Table 1. *Mechanical Properties of the Experimental Material*

Specimen No.	Dimensions of the cross-section, mm		σ_y MPa	σ_{UTS} MPa	Elongation %
	thickness	width			
1	2.01	12.53	525	602	11.2
2	2.01	12.53	530	601	12.6
7075-T6 SAE J454	1/16"		503	572	11.0

Obtained results exhibit relatively high strength and somewhat limited plasticity of the experimental material. By the fractography analysis of the fracture surfaces performed by the JSM JEOL 840 scanning electron microscope (SEM) laminated morphology of the fracture surface was observed (Fig. 1a). At higher magnifications the transgranular dimpled fracture was found within the layers whereas on the interlayer boundaries deep tears are observed (Fig. 1b).

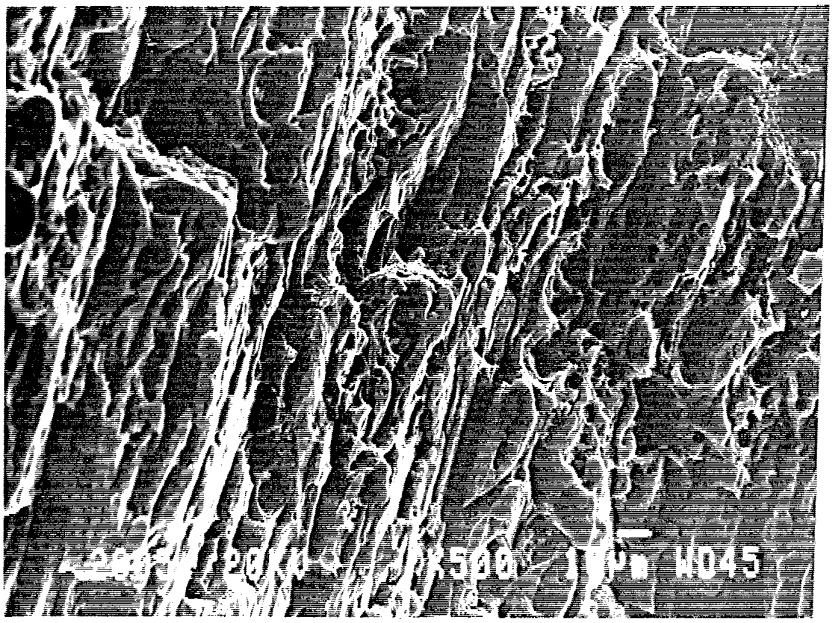

a

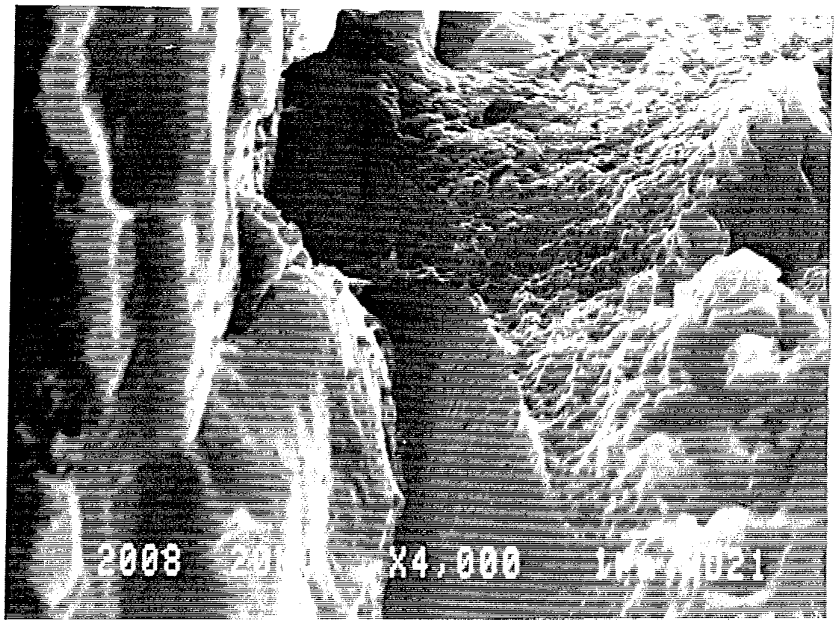

b

Fig. 1. Appearance of the fracture surface of the tensile specimen. SEM.
a. Laminated fracture surface. (arrow 1) Magnification: × 500
b. Transgranular dimpled and intergranular fracture patterns.
(arrow 2) Magnification: × 400

2.2 Specimens

The multicrack specimen is a rectangular thin sheet panel with two identical rows of evenly spaced edge crack starters (one row on each side) generating in the course of the loading two arrays of parallel edge cracks. Schematic representations of the multicrack specimen with eight cracks, used in this study is given in Fig. 2. The prenotch (crack starter) depth was 3 mm (except one specimen with 2.5 mm notch depth).

Specimen dimensions and intercrack spacing were chosen so that the crack interaction could be considered as negligible for the crack lengths up to 13 mm (3 mm crack starter and 10 mm actual crack length). In order to keep the interaction effect on strain intensity factor (SIF) lower than 2% the intercrack spacing was chosen to be 200 mm. A pin-hole flat grips fastened by 7 bolts to the specimen have been coupled with the spherical hinge installed in the Instron frame in order to provide axiality of loading.

Attachment of the grips to the specimen was performed with great care and the nonaxiality of grips pinhole relative to the specimen axes did not exceed 0.25mm. The uniformity of stress distribution within the transverse cross-section was monitored via 6 strain gauges attached in two rows on two levels: between the first and the second rows of cracks as well as between the third and the fourth crack rows. Each row of strain gauges comprises two edge gauges (one at each edge) and one central gauge. This arrangement enabled verification of the stress uniformity over the specimen before the test and continuous monitoring of the stresses during the test.

A general view of the experimental set-up is shown in Fig. 3. It should be noted that for the upper and lower cracks the distance to the grips edge is as important as the intercrack spacing. Since the grips have much higher stiffness than the specimen they constrain transverse deformation of the specimen causing disturbance of the stress field at the grip edges.

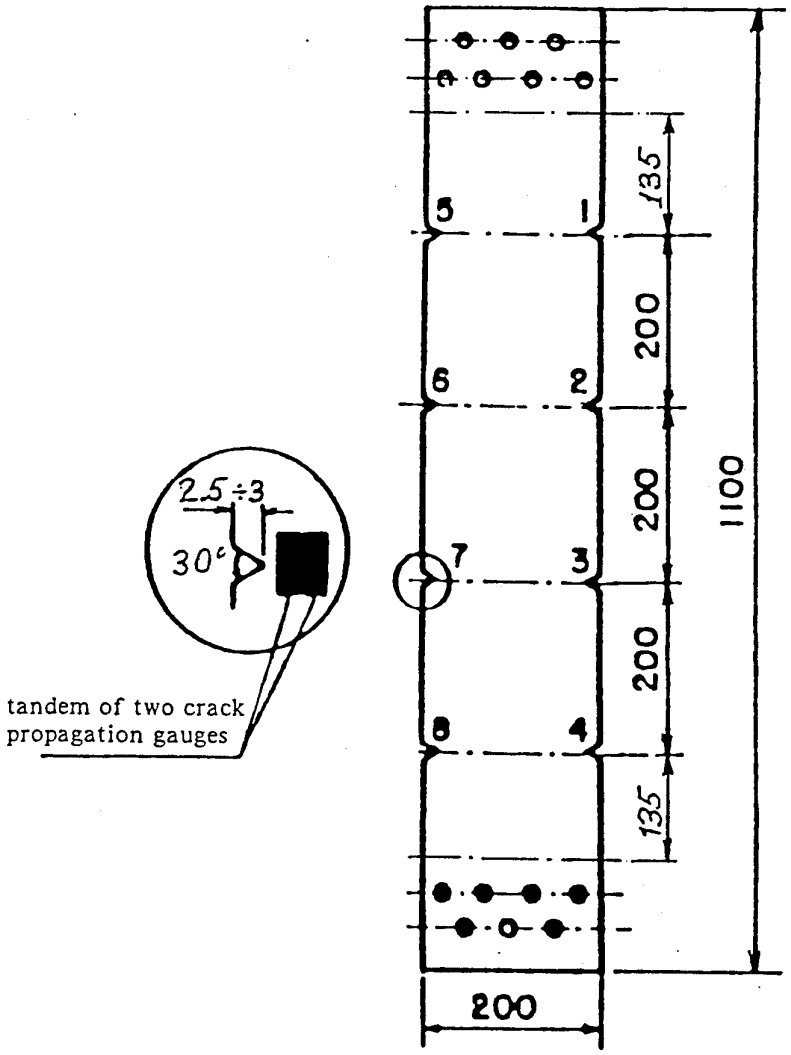

Fig. 2. Schematic representation of the "multicrack" specimen with eight side notches (crack starters)

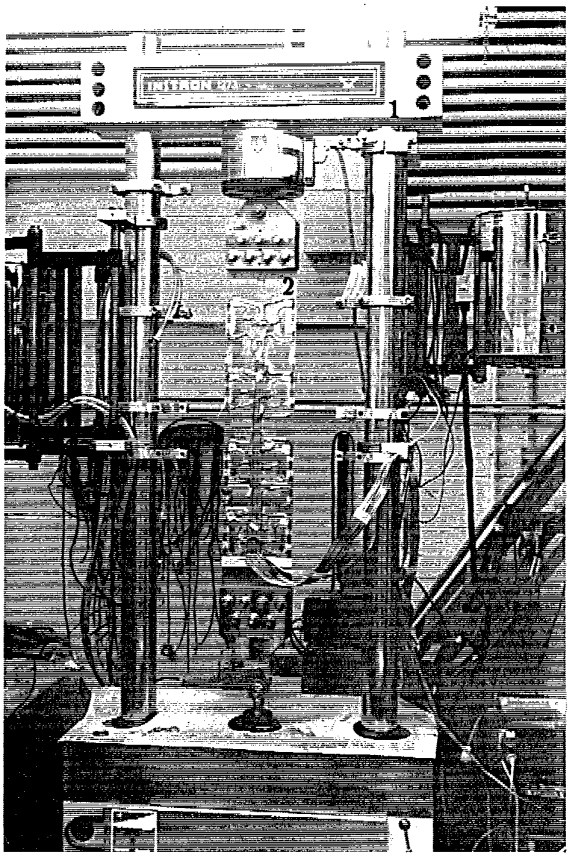

Fig. 3. General view of the experimental set-up.
1. Instron frame
2. Multicrack specimen

Fig. 4 shows FEM*-calculated stress distribution in the specimen (near the grips) loaded by a nominal stress of 50 MPa. As can be seen from the above plot the total attenuaion of the stress field disturbance is observed on the distance of 250-300 mm from the grips edge. Since the distance from the extreme cracks to the grips is 135 mm a 2% decrease of the stresses could be expected at the specimen edges. On the contrary the 2% increase of the stresses could be expected in the specimen centre. These values of the stress disturbance could be considered as negligible.

The edge notches were prepared by milling with wedge shaped tool (wedge angle 30°). Crack propagation gauges of Kyowa KV-5C type with 4.6 mm width and 0.1mm distance between the strands were used for measuring the fatigue crack growth rate. The gauge consists of a number of resistor strands connected in parallel. The tandem of two gauges attached at each notch (the first gauge close to the notch tip and the second gauge at the distance of 0.4÷0.6 mm from the first gauge). Progression of the crack through the gauge pattern causes successive cutting of the strands, resulted in increase of the gauge resistance which is recorded by the measuring system, in a form of a sequence of step-wise signals.

2.3 Description of the experimental system

The block-diagram of the experimental system developed for the testing of the multicrack sheet specimens is shown in Fig. 5. It is based on the closed loop hydraulic Instron testing machine (1) with load cell (2), LVDT (3) and extensiometer (4) for measurement of load, position and crack opening displacement respectively. The system includes:

- specimen (5) containing propagating cracks and gauges for measurement of the crack length and the strains, respectively;

- two grips (6) for fastening the specimen and its installation in the Instron machine (1);

- control block (7) of the Instron machine;

---

*FEM - Finite Element Method.

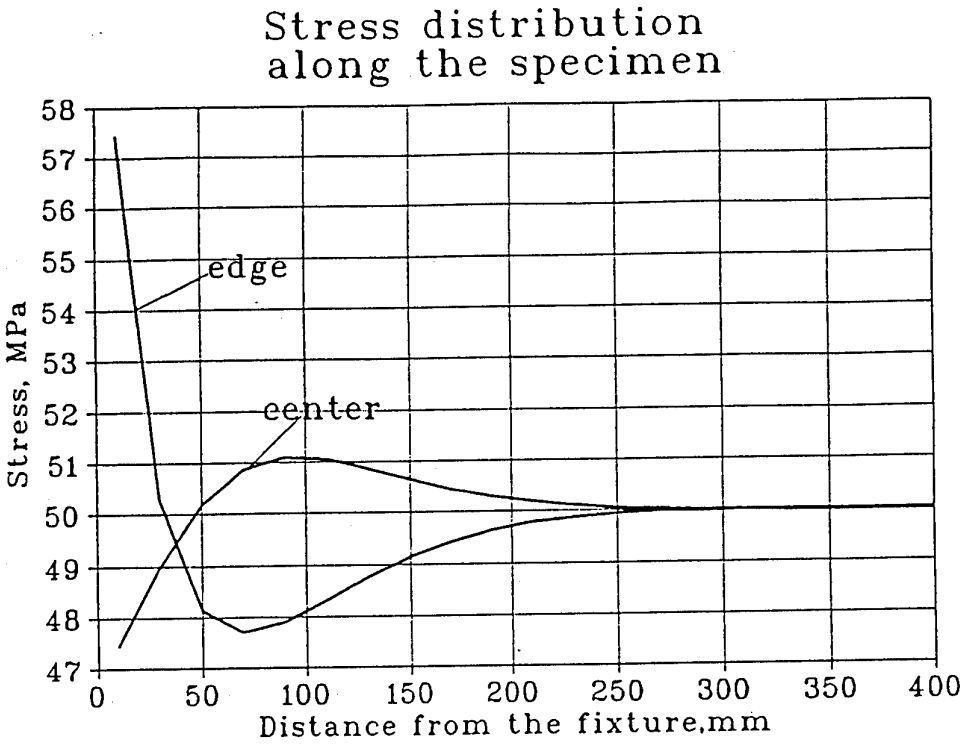

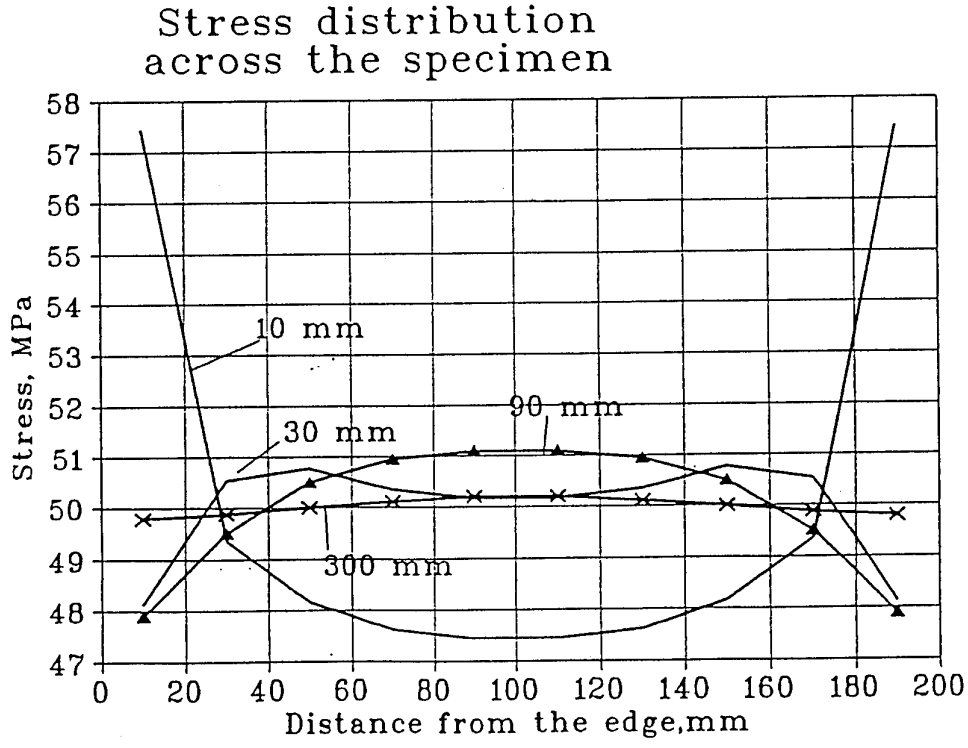

Fig. 4 Stress distribution along and across the specimen near the grip calculated for nominal stress of 50 MPa

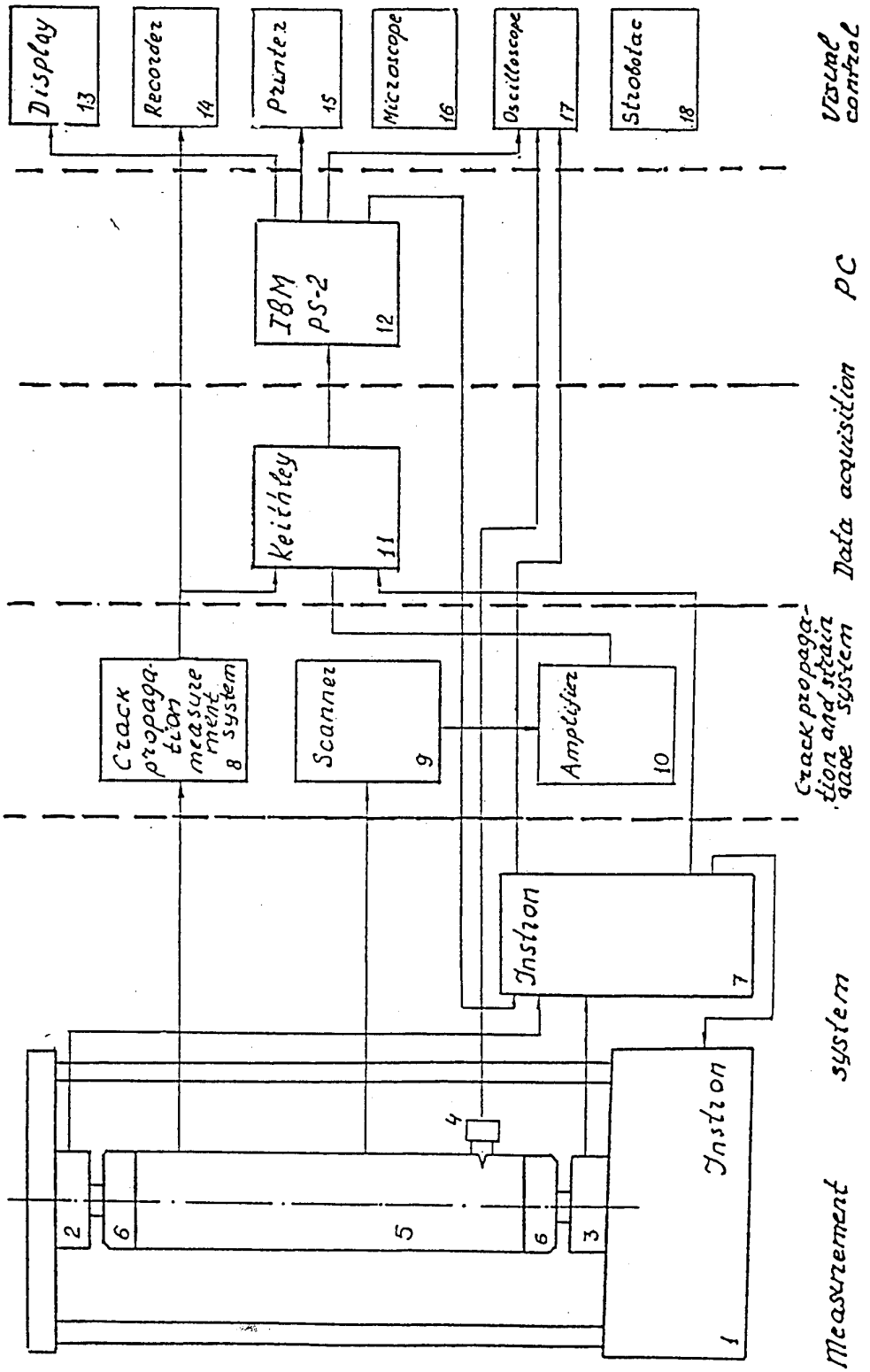

Fig. 5 The block diagram of the testing system

- multichannel crack propagation measurement system (8);

- Keithley 500A system (11) for A/D and D/A conversion, data acquisition and processing;

- 10 channel scanner (9) for successive switching the strain gauges to the strain gauge amplifier (10);

- IBM PS/2 computer (12) for generation of the load signals (fed to the load controller of the Instron machine (7)), and for data acquisition, processing, displaying and storing;

- oscilloscope (17) and recorder (14) for visual monitoring of the chosen signals;

- microscope (16) and stroboscope (18) for visual observation of the crack growth during the test.

2.4 Crack propagation measurement system

The crack propagation measuring system is based on the Kyowa crack propagation gauges of KV-5C type, includes an electronic circuit and a power supply. As was mentioned above the crack propagation gauges have a grid which consists of 46 resistor strands spaced by 0.1 mm and connected in parallel. For extension of the measurement range up to 10 mm two gauges are used in tandem. The details of measuring procedure are given below. The output signal from the crack propagation gauge has a step-wise form so that each step caused by the strands cutting indicates a 0.1 mm crack increment.

In an original application the crack propagation signal has non-equal steps increasing with crack growth due to the diminishing number of the strands still remaining unbroken. This makes the crack growth data analysis somewhat cumbersome. To preserve equality of all the steps an improvement has been introduced in the crack propagation measuring system (Fig. 6). The steps equality is provided using two resistors R1 and R3 connected with the first crack propagation

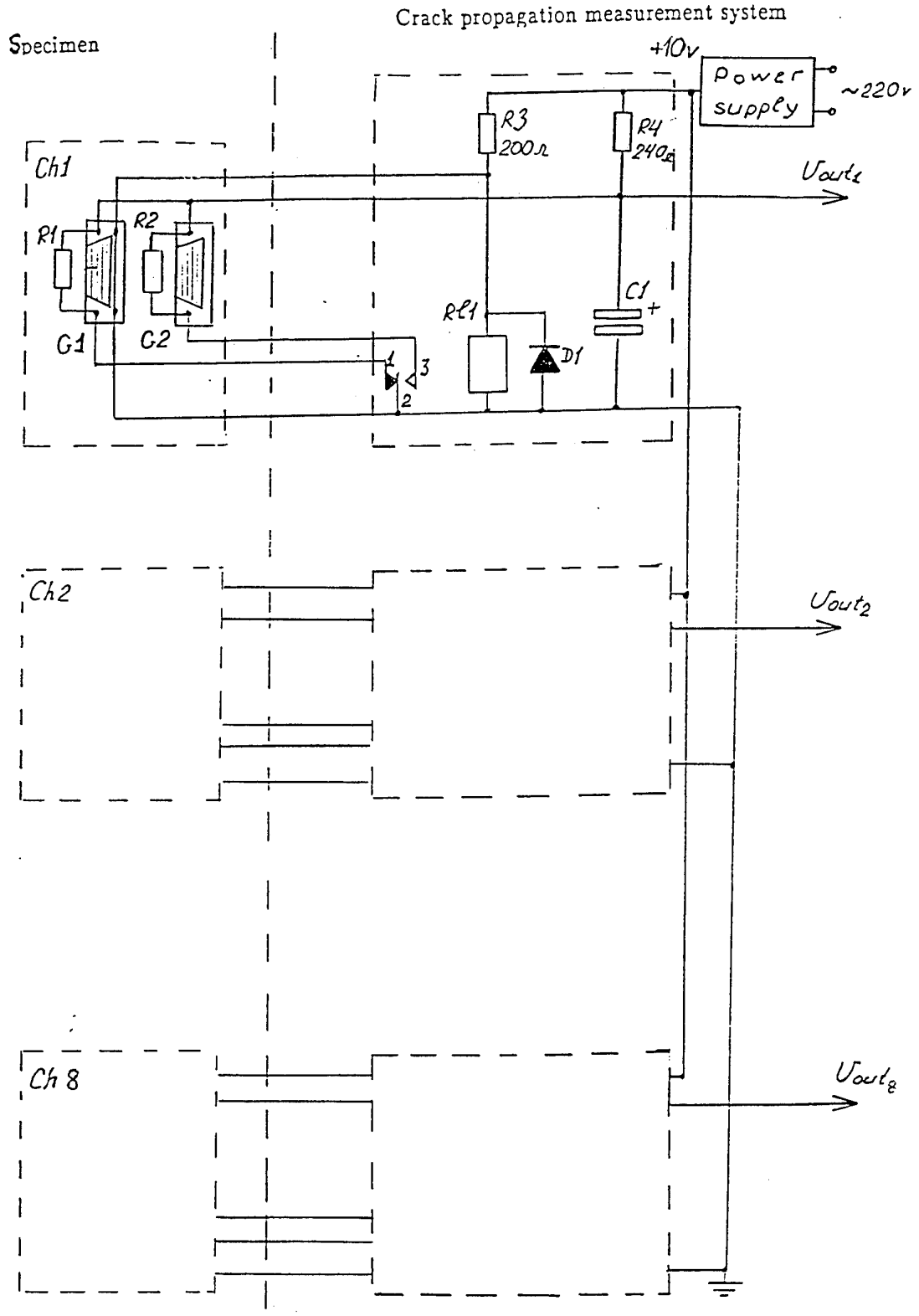

Fig. 6. Electrical circuit of the crack propagation measurement system

gauge G1 in parallel and in series, respectively. The resistors R2 and R4 play the same role for the second crack propagation gauge G2. Using the 10V power supply the almost constant voltage steps of about 0.5 mV were achieved, thus facilitating significantly the crack length measurement and data analysis.

The extra strand located at the end of the KV-5C crack propagation gauge is used to switch the circuit from the first crack propagation gauge G1 to the second G2. The above mentioned extra strand on the G1 gauge shunts the coil of a reed relay Rℓ1. The contacts 1 and 2 of Rℓ1 are normally closed and the output voltage corresponds to the G1.

When the crack cuts the extra strand of the G1 the voltage drop on the Rℓ1 coil increases. As a result Rℓ 1 switches, causing the contacts 2-3 to be closed and output voltage to be measured from the G2 gauge. The example of the plot recorded by one of the crack propagation channels is shown in Fig. 7.

2.5 The 10-channel scanner

The scanner provides successive connecting with the amplifier of the half bridge circuits associated with the strain gauge attached to the specimen. It consists of up to ten identical electrical circuits. Each of these circuits consists of the input amplifier and reed relay. The amplifier is compatible with 5V Keithley 500A data acquisition system. The control of the scanner is performed by digital signals from the Keithley system which are exitated by the adequate computer commands.

The strain gauges (arranged in a half-bridge) are automatically connected to the measuring scheme as far as the Keithley control digital signal is 1, and disconnects - if the signal is 0.

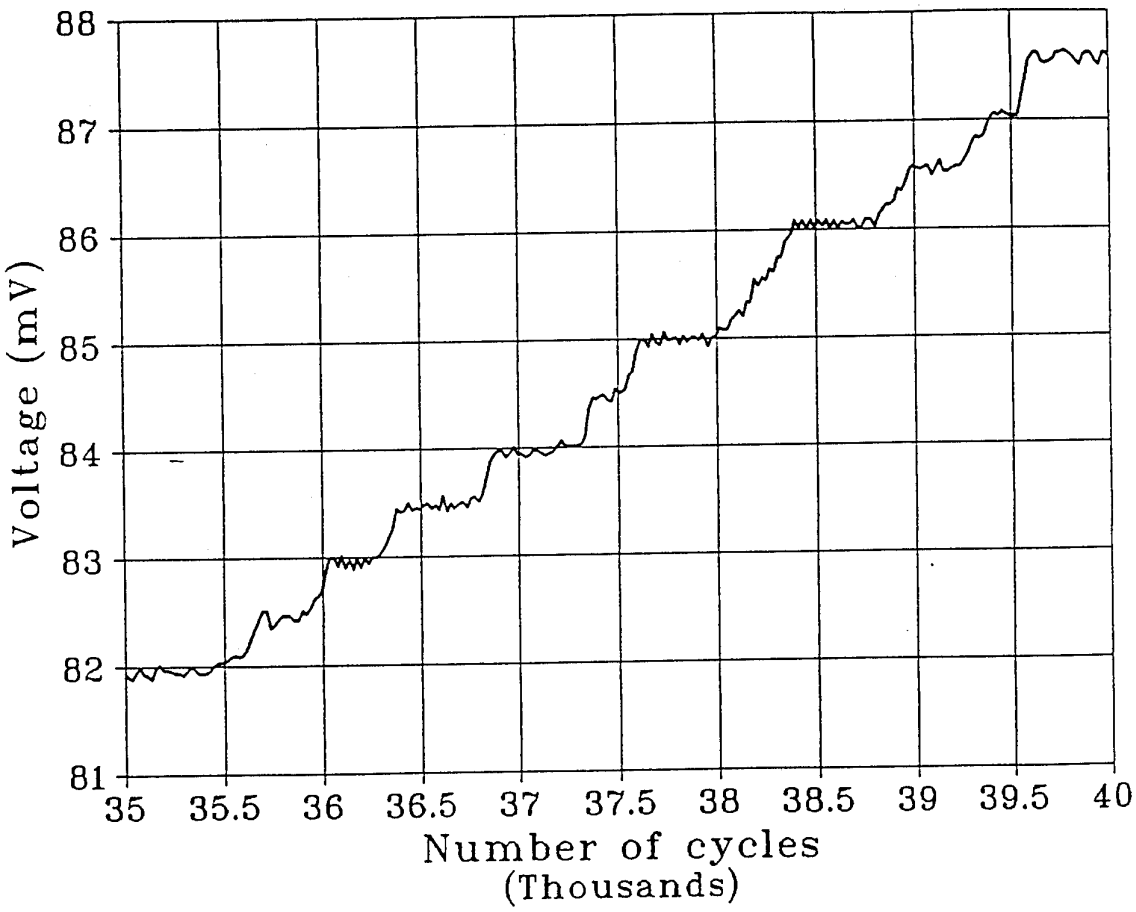

Fig. 7. Segment of a crack propagation record

2.6 The strain gauge amplifier

The strain measurement is based on the Kyowa strain gauges KFG-5 with gauge length 5mm, gauge resistance 120 ohm, gauge factor about 2.2 and with temperature compensation corresponding to the aluminium alloys. Each strain gauge is connected with "dummy" gauge in the Wheatstone half bridge circuit for increasing temperatures stability of measurements.

The amplifier provides an adjustable amplification coefficient (up to 10^4) of the low level direct current signals from the Wheatstone half bridges, adjustable offset for zero suppression, calibration and checking of the amplification coefficient and signal reading by the 4 digital light emitter diode display.

3. Development of the Software for Multi-Crack Fatigue Tests

3.1 General Structure of the Software

Multi-crack fatigue tests were performed under different kinds of loading:

- sine wave cyclic loading with given constant frequency and amplitude (CA);
- the above cyclic loading with superimposed overloads (CAO) ;
- the succession of random amplitudes combined by sine wave form;
- the above random loading with superimposed overloads.

For performance of these types of experiments a computer controlled testing system was developed including special software. This software performed the following functions:

- elaboration of the control signal for monitoring the base-line cyclic loading;
- setting the loading parameters from the computer keyboard;
- generation of the random loading;
- generation of the overloads of various magnitude;
- acquisition of the strain gauges data;

- acquisition of the crack propagation gauges data;
- acquisition of the load and LVDT (position) data via Instron testing machine controller;
- permanent exhibition of the acquired data on the monitor display;
- processing of the test data.

Most of the above tasks are carried out in the real-time mode. Because of the limitations imposed by the testing procedure and data acquisition system the cycle frequency was limited to 5 cycles per sec. Due to the computer memory limitations the rate of the data acquisition from the crack propagation gauges was limited to one per 20 load cycles. The crack propagation gauges signals and the other output test data were displayed on the monitor - one per 40 load cycles.

3.2 Software for random fatigue loading generation

Software that was developed for generation of the random fatigue loading, performs the following functions:

- generation of a Gaussian stationary random process;
- filtering (reduction) of the generated load history in order to exclude the small load oscillations, which don't influence the fatigue damage. The filtering leads to reduction of the total testing time (test acceleration);
- real-time control over the random loading performed by the Instron machine.

The first part of the software written on the C programming language carries out generation of a Gaussian stationary random process in accordance with a preselected autocorrelation function by the method of the sliding summation [5]. The outline of the method is given below.

Let $x(t)$ be a stationary Gaussian stochastic process with the mean value $M(x(t))=0$ and standard deviation $\sigma(x(t)) = 1$. The common case may be easily obtained by linear conversion of this process. For an ergodic process the autocorrelation function can be derived from a single realization of the process:

$$K(t) = M(x(\tau)*x(t+\tau)), \quad (1)$$

where M stands for integration over τ in the infinite interval.

The power spectrum density is expressed by the Fourier transform of the correlation function:

$$S(\omega) = 1/(2\pi)*\int_{-\infty}^{\infty}(\exp(-i\omega\tau)*K(\tau)*d\tau \quad (2)$$

The method of the sliding summation is based on representation of the random process in the form:

$$x(t) = \int_{-\infty}^{\infty} g(\tau)N(t-\tau)d\tau, \quad (3)$$

where

N(x) is the standard "white noise" - independent and uniformly distributed in the interval [0,1] random values,

$g(\tau)$ is a filter function, which may be expressed through the power spectrum function:

$$g(\tau) = 1/(2\pi)*\int_{-\infty}^{\infty}\sqrt{S(\omega)}\ \exp(i\omega\tau)d\tau \quad (4)$$

Rewriting the expression (3) in discrete form, we receive

$$x(k) = \sum_{j=-M}^{M}\sqrt{\delta t}*g(j\delta t)*N(k-j), \quad (5)$$

where

δt is the time interval between two successive moments

M is a number of the time intervals for a time greater than the radius of correlation.

Autocorrelation function, corresponding to the characteristics of the service loading, was chosen as follows:

$$K(\tau) = \exp(-1.35*|\tau|)*\mathrm{Cos}(2\tau) \quad (6)$$

Example of the loading history generated using the above procedure is shown in Fig. 8. For verification of the developed procedure the autocorrelation function of the simulated history was calculated according to the formula (1). As can be seen from Fig. 9, the calculated autocorrelation function is sufficiently close to the initial autocorrelation function, thus demonstrating good quality of generation procedure.

The second part of the software contains programs, written on the QUICK-BASIC language, which perform filtration of the generated loading history so that the resulting loading history does not contain ranges with amplitudes smaller than a given threshold level.

Algorithm of the program, that executes "reduction" of the simulated loading history with a given threshold value, can be presented as follows:

1. Let us consider three successive reversals. If the absolute difference between the first and the second reversals is greater than the given threshold, the first reversal should be rewritten to the "reduced" file. Then the new reversal value is extracted from the source file for the further treatment.
2. If the above-mentioned difference is smaller than the given threshold, two reversals from the current three are discarded in the following way:
   - the first and the second reversals are discarded, if the absolute difference between the third and the second reversal is greater than that between the second and the first;
   - the second and the third reversals are discarded in the opposite case.
3. Two following reversals are extracted from the source file and the treatment repeats.

This step-by-step procedure is performed until all the reversals are checked up to the end of the file.

The "reduced" loading history consists only of cycles with ranges greater than the given threshold.

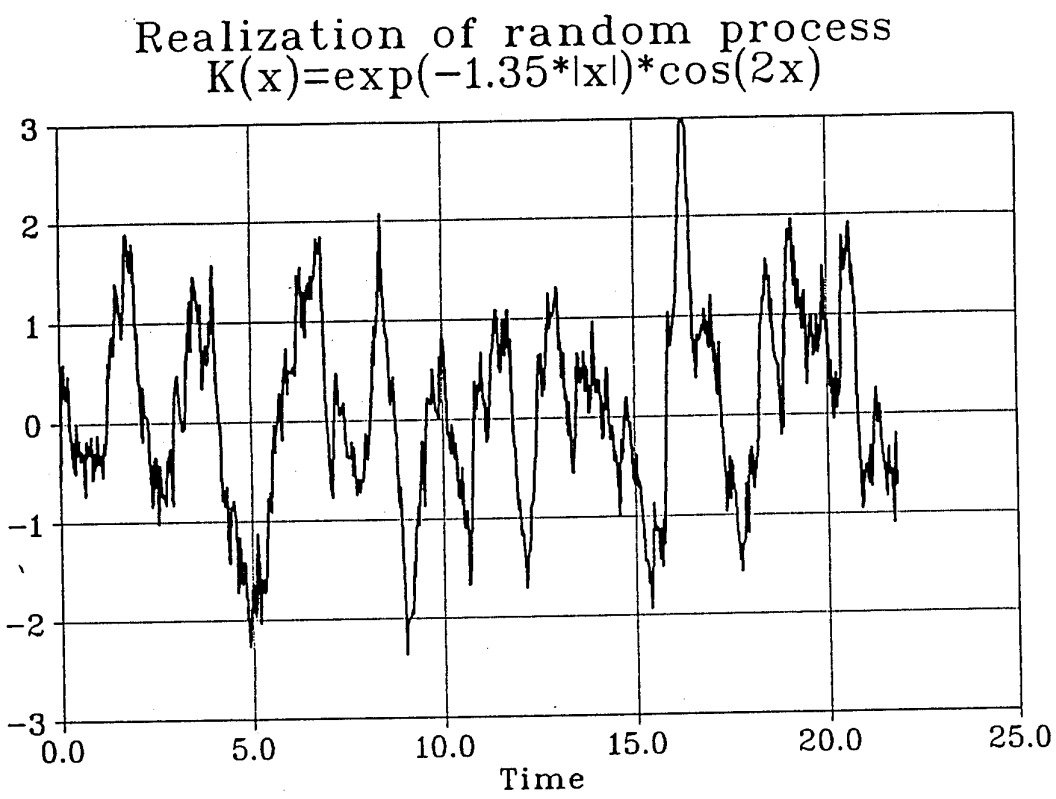

Fig. 8. A segment of the generated random process

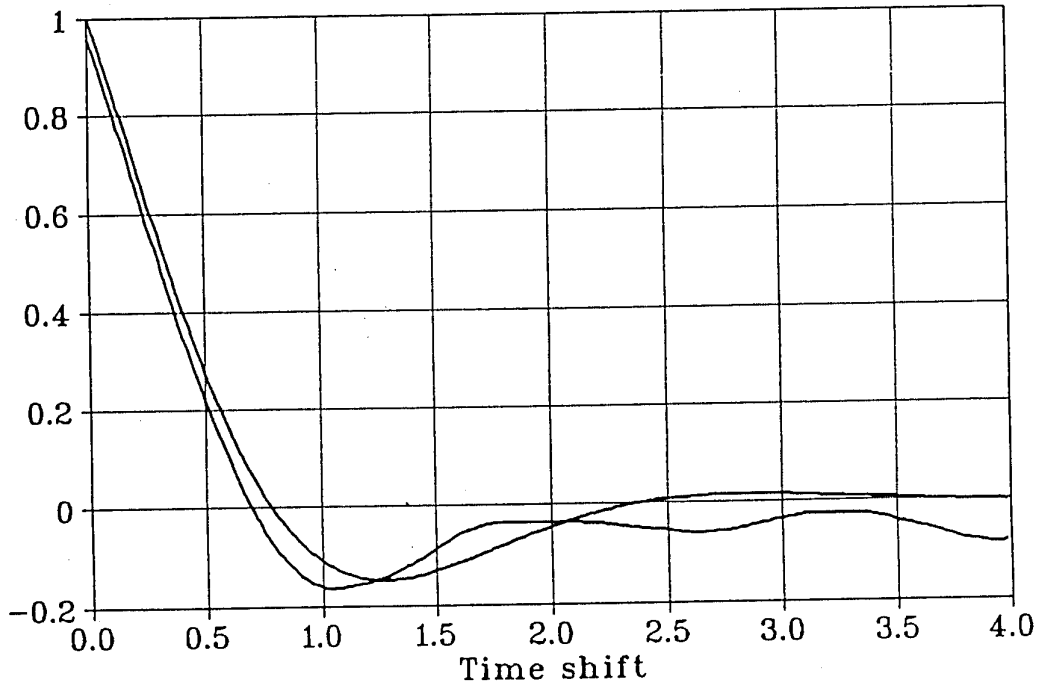

Fig. 9. Auto-correlation function of the random process
1 - the initial function
2 - the auto-correlation function calculated on the basis of the generated process

In the Fig. 10 two "reduced" loading histories are shown, which are obtained by elimination from the initial loading history (Fig. 8) the cycles with amplitudes smaller than a half or one standard deviations of the random process respectively.

The obtained "reduced" loading history may be fed into the controller of the Instron machine. But the method of the direct using of the generated and the "reduced" loading history has the following shortcomings. Firstly, the obtained loading history has a limited length, so it should be repeatedly used for a long life time. Secondly, the loads follow in a strict order for all the tests. Both of the above shortcomings limit the randomness of the loading history.

To overcome these shortcomings the following procedure for generation of a variety of the loading histories based upon the sole generated and loading history and its filtered variations was developed. The overall load interval, which is assumed to be confined by ± 4.5 of the standard deviations, is divided into 18 subintervals. The load ranges from one reversal to the next one are counted for all combinations of the subintervals. As a result a transition probability (frequency) matrix is obtained. This matrix is used for the real-time generation of a random reversal succession during the test. The successive reversals are combined with the half sine segments of constant cycle frequency. This makes the load monitoring and data acquisition more convenient.

Two transition frequency matrices have been obtained for "reduced" loading histories: one with the threshold value equal to one and the second to two standard deviations. The latter matrix is given in the Table 2. Every element in the transition frequency matrix corresponds to the accumulated frequencies of the reversal transitions from a load level corresponding to a column number j to the load level corresponding to the row number i.

The accumulated frequencies for the descended transitions are represented to the right of the main diagonal, whereas the accumulated frequencies for the ascended

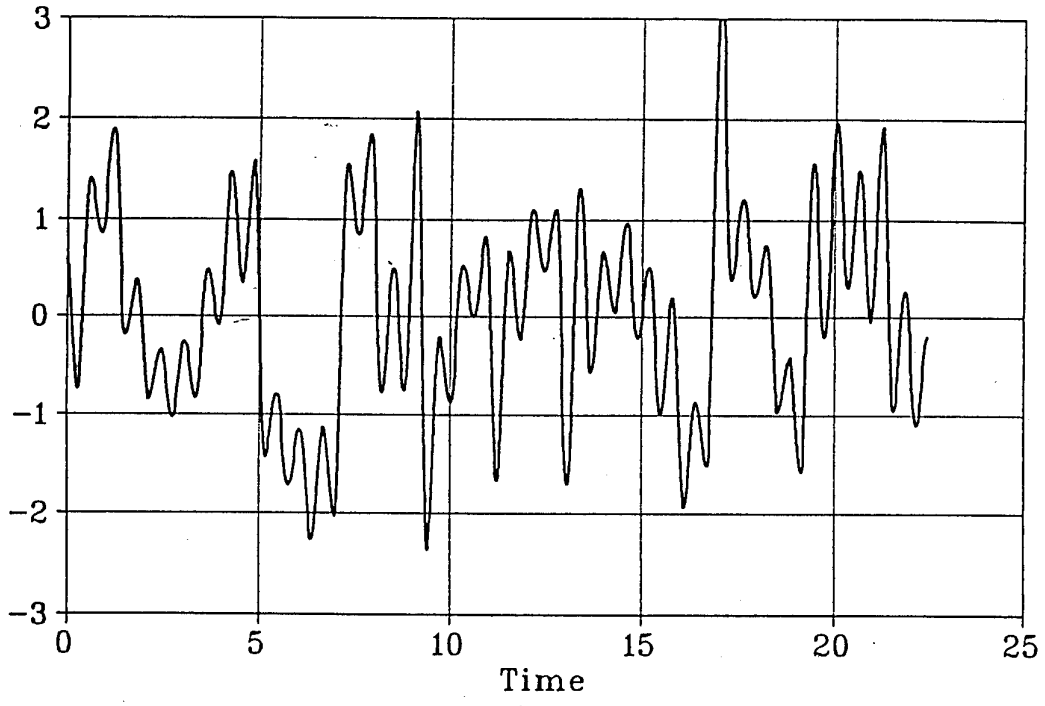

a

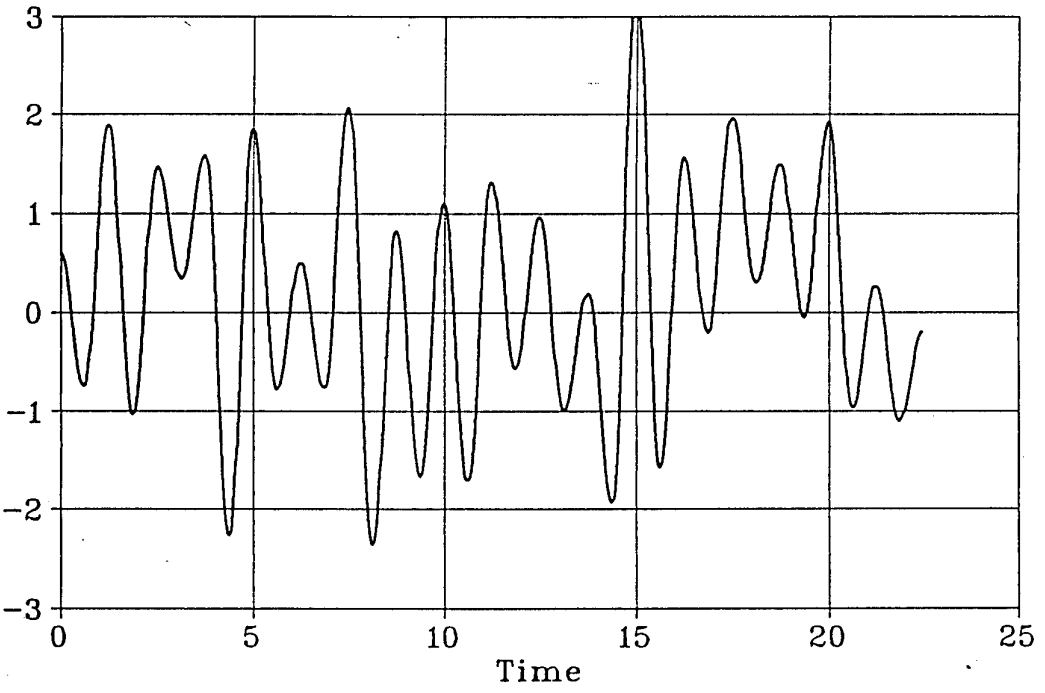

b

Fig. 10. Results of elimination of the ranges smaller than a half of standard deviation (a) and one standard deviation (b) from the segment of the initial random process shown in Fig. 8.

Table 2. Accumulated transition frequency matrix

P max	P min					
	Divisions					
Div.	1	2	3	4	5	6
1	xxx	0	0	0	0	0
2	0	xxx	0	0	0	0
3	0	0	xxx	0	0	0
4	0	0	0	xxx	0	0
5	0	0	0	0	xxx	0
6	0	0	0	0	0	xxx
7	0	0	0.00361	0	0	0
8	0	0	0.00722	0.00219	0	0
9	0	0	0.01444	0.01319	0.00892	0
10	0	0.01887	0.05776	0.04725	0.06049	0.03815
11	0	0.11321	0.15523	0.17363	0.18989	0.19011
12	0.25	0.28302	0.42238	0.38242	0.42687	0.44488
13	0.41667	0.49057	0.68231	0.66264	0.69311	0.71128
14	0.58333	0.84906	0.87004	0.85275	0.87605	0.89719
15	0.91667	0.96226	0.96751	0.95275	0.96331	0.97026
16	1	0.98113	0.99639	0.98462	0.99058	0.99515
17	1	1	1	0.9989	0.99851	0.99968
18	1	1	1	1	1	1

Table 2. Continuation

P max	P min					
	Divisions					
Div.	7	8	9	10	11	12
1	0	0	0	0.00376	0.00083	0.00116
2	0	0	0.03333	0.01128	0.00578	0.00427
3	1	0	0.1	0.03759	0.03138	0.02521
4	1	1	0.3333	0.16541	0.11643	0.10512
5	1	1	1	0.57143	0.35178	0.29635
6	1	1	1	1	0.75557	0.59581
7	xxx	1	1	1	1	0.89876
8	0	xxx	1	1	1	1
9	0	0	xxx	1	1	1
10	0	0	0	xxx	1	1
11	0.12768	0	0	0	xxx	1
12	0.4237	0.25119	0	0	0	xxx
13	0.71971	0.64129	0.44611	0	0	0
14	0.90567	0.86013	0.78814	0.48649	0	0
15	0.97278	0.95718	0.95911	0.78378	1	0
16	0.9931	0.99429	0.99628	0.94595	1	0
17	0.99808	1	1	1	1	0
18	1	1	1	1	1	0

Table 2. Continuation

P max	P min					
	Divisions					
Div.	13	14	15	16	17	18
1	0.00099	0.00049	0.00231	0	0.01492	0
2	0.00599	0.00595	0.01043	0.00358	0.04478	0
3	0.03296	0.03474	0.04971	0.01792	0.08955	0.2
4	0.11318	0.12605	0.16301	0.10753	0.20896	0.3
5	0.29028	0.29578	0.35491	0.32258	0.34328	0.5
6	0.56125	0.57866	0.60694	0.67384	0.59701	0.7
7	0.82324	0.81042	0.84509	0.87455	0.79104	0.9
8	0.96505	0.93747	0.93064	0.95341	0.97015	0.9
9	1	0.98859	0.98613	0.98925	1	1
10	1	1	0.99884	1	1	1
11	1	1	1	1	1	1
12	1	1	1	1	1	1
13	xxx	1	1	1	1	1
14	0	xxx	1	1	1	1
15	0	0	xxx	1	1	1
16	0	0	0	xxx	1	1
17	0	0	0	0	xxx	0
18	0	0	0	0	0	xxx

transitions to the left of the main diagonal. Each column in the matrix may be considered as an accumulated frequency function F(i,j) for transition from an initial value (corresponding to the column number j) to the target values (corresponding to the row numbers less than i). The difference between two adjacent (i and i-1) values in the column forms the differential transition frequency from the j-load value to the i-load value.

The random loading is realized, using above-mentioned two-dimensional transition frequency matrix (Table 2), as follows.

Two random numbers X1 and X2, both uniformly distributed in the interval [0,1], are computer generated on every step of the program execution.

Let us consider a load minimum corresponding to the k-th matrix division. The following load maximum corresponds to the l-th division, if

$$F(\ell,mk) > X1 > F(\ell-1,k)$$

where $F(\ell,k)$ and $F(\ell-1,k)$ - values of the accumulated frequencies corresponding to the ℓ and $\ell-1$ divisions. The next load minimum will be obtained using the second random number due to the condition

$$F(m,\ell) > X2 > F(m-\ell,1),$$

as corresponding to the m-th load division.

In accordance with the obtained maximum and minimum load values (l and m) program defines the two half sine wave forms connecting the three versals (k, ℓ and m) and sends them to the Instron machine control block.

Generated random process can be characterised by a number of statistical parameters. One of such parameters is the irregularity factor γ, being the ratio of zero crossings number to the reversals number. This parameter characterises the degree of the narrow-band property of the process spectrum and it influences the "fatigue damage ability" of the loading process. The γ-value for the generated process was determined numerically by counting the number of the zero crossings, as well as the number of reversals along a

predetermined segment of the loading history.

The number of reversals within the above segment was found to be 812,521 whereas the number of zero crossings was 108,225. Thus, the irregularity factor γ is 0.133. This value is characteristic of the wide-band random process. After filtration, i.e., after elimination of the reversals smaller than two standard deviations of the process the number of reversals within the same segment was 20,647 and the number of zero crossings was 20,501, i.e., the γ-value was found to be 0.993. Such γ-value is characteristic of the narrow-band random process.

It is believed that the most adequate procedure for assessment of "damage ability" of the random loading process is the rain-flow analysis. This analysis includes determination of the two-dimensional distribution of the rain-flow cycle maxima and minima. The numerical procedure used for these purposes was in accordance with the algorithm given in ASTM E 1049-85 standard [6]. The range of load alterations confined by ± 4.5 standard deviations of the process was subdivided in 18 divisions, whereas the extremely rare excursions of the processes beyond the above range were incorporated within the extreme divisions. The results of numerical calculations performed using the above-mentioned filtered segment of the process (with two standard deviation elimination thresholds) are presented in Table 3. The rainflow cycles maxima, minima and ranges distributions can be easily obtained from the two-dimensional matrix of Table 3 by summation along the rows, columns and diagonals, respectively.

These distributions are presented in graphical form in Fig. 11.

4. Results of the Fatigue Crack Growth Tests

4.1 Crack growth under CA-cyclic loading

Two multicrack specimens (No. 1 and No. 2) were used for investigation of fatigue crack growth under CA-loading. The specimen No. 1 was actually used for the running-in of the test procedure and determination of the loading cycle

Table 3. Results of the rain-flow cycle counting

P max	P min								
	Divisions								
Div.	1	2	3	4	5	6	7	8	9
1									
2									
3									
4									
5									
6									
7			1						
8				3					
9				5	25				
10				4	88	174			
11			2	19	150	548	492		
12			6	51	276	775	1032	438	
13			11	135	560	904	747	465	181
14	1	3	40	293	616	543	281	130	77
15		6	95	286	255	139	53	14	11
16		21	98	98	44	10	3	4	
17	6	20	23	15	2	1			
18	4	3	1	1	1				

Table 3 Continuation

P max	P min								
	Divisions								
Div.	10	11	12	13	14	15	16	17	18
1									
2									
3									
4									
5									
6									
7									
8									
9									
10									
11									
12									
13									
14	31								
15	5	1							
16	1								
17									
18									

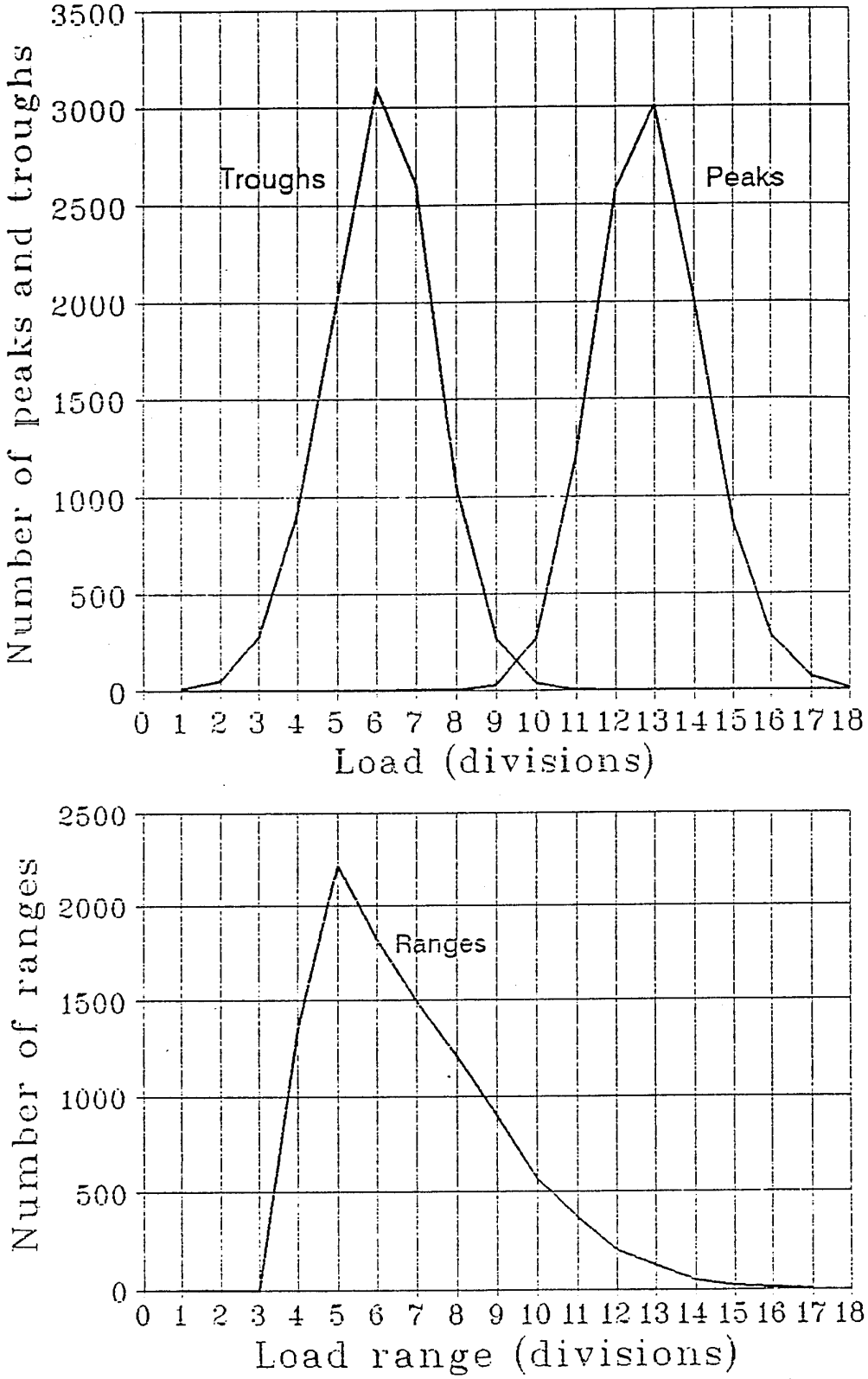

Fig. 11. Rain-flow cycle maxima (peaks), minima (troughs) and ranges distribution (The generated random process after elimination of the ranges smaller than 2 standard deviations)
Each division is equal to 0.5 standard deviation.

parameters. The specimen No. 1 was the only specimen with the prenotches depth 2.5mm (the others had the prenotches depth 3 mm). The test was started under the following cycle parameters: Maximal cyclic load, P_{max}=49000N, minimal cyclic load, P_{min}=9800N. The corresponding nominal stresses related to the gross cross-section of the specimen were σ_{max}=122.5MPa and σ_{min}=24.5 MPa respectively. This conditions proved to be too damaging since already after 13000 cycles the first cracks appeared at the crack starter notches.

In order to decrease crack propagation rate the minimal cyclic load was raised up to 19600N thus reducing significantly the cycle amplitude. Since the crack rate decrease was not sufficient, after 20000 cycles from the beginning of the test the minimal cycle load was raised to 29400N, thus additionally decreasing the cycle amplitude. These loading parameters corresponding to the following nominal cyclic stresses: σ_{max}=122.5 MPa, σ_{min}=73.5MPa and σ_a=24.5 MPa, were kept up to the end of the test (here σ_a is the amplitude of the cyclic stresses).

Based on the experience acquired during the test of the specimen No. 1 the following parameters of the loading were adopted for the specimen No. 2: P_{max} = 39200N, P_{min}=19600N, i.e., σ_{max}=98MPa, σ_{min}=49MPa and σ_a=24.56 MPa. These parameters were kept unchanged during the whole test.

The treatment of the experimental data included several steps. First of all the initial data acquired by computer was analysed. This initial data represented the changes of the voltage outputs of the crack propagation gauges, firstly, on the first gauge and, afterwards, on the second gauge in the tandem (Fig. 12). Each step on the initial plot represents the gauge strand crossing by the growing crack. Since the interstrand spacing is constant and equal to 0.1 mm the crack rate can be easily determined. Knowing the distance of the first strand in the first crack propagation gauge from the specimen edge the above plot can be easily rearranged to give a curve depicting the crack length as a function of the cycles number. Figs. 13 and 14 show the crack growth plots for the specimens No. 1 and No. 2, respectively.

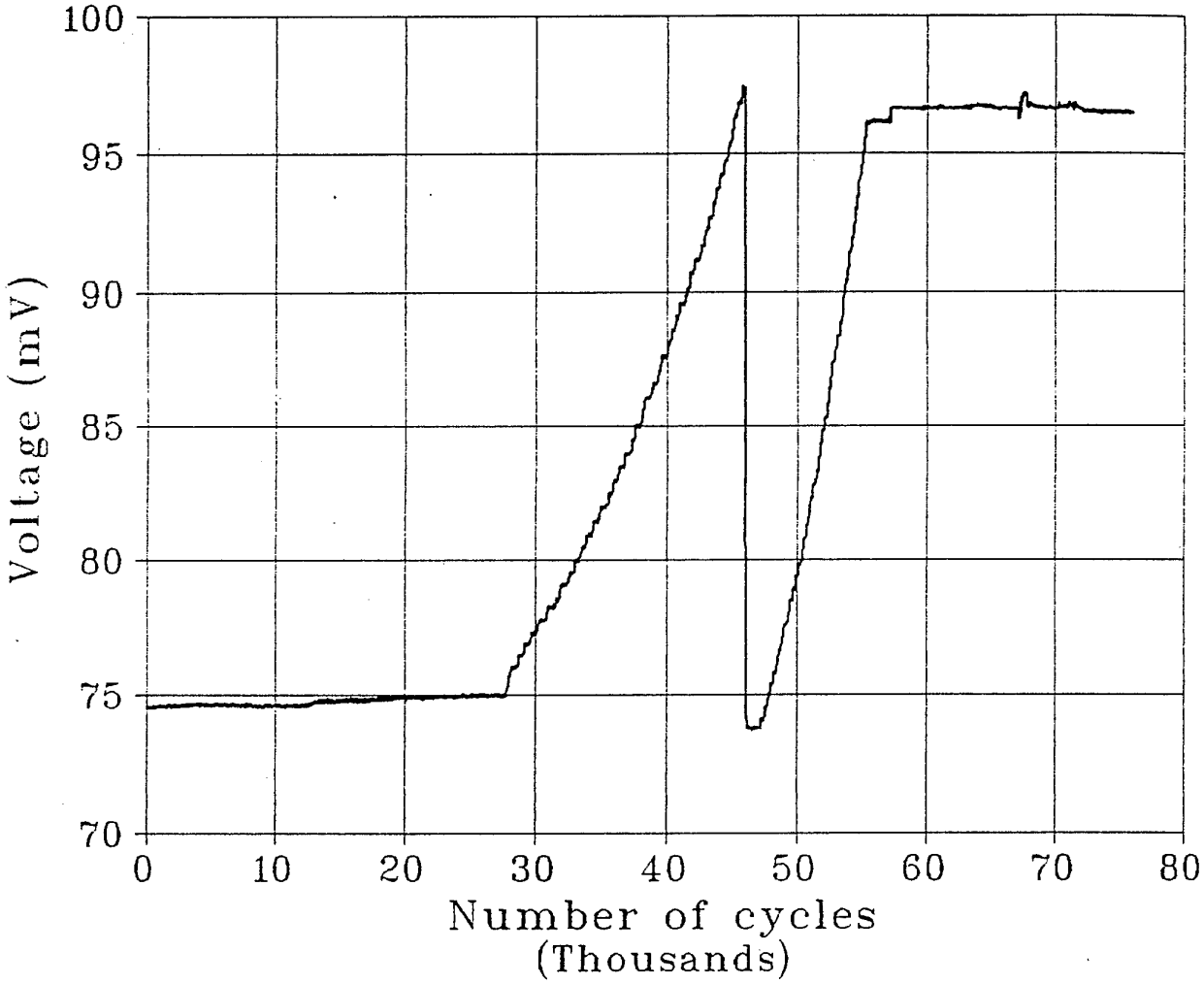

Fig. 12. Original plot of the crack growth.

1. Crack growth curve corresponding to the first crack propagation gauge
2. Crack growth curve corresponding to the second crack propagation gauge

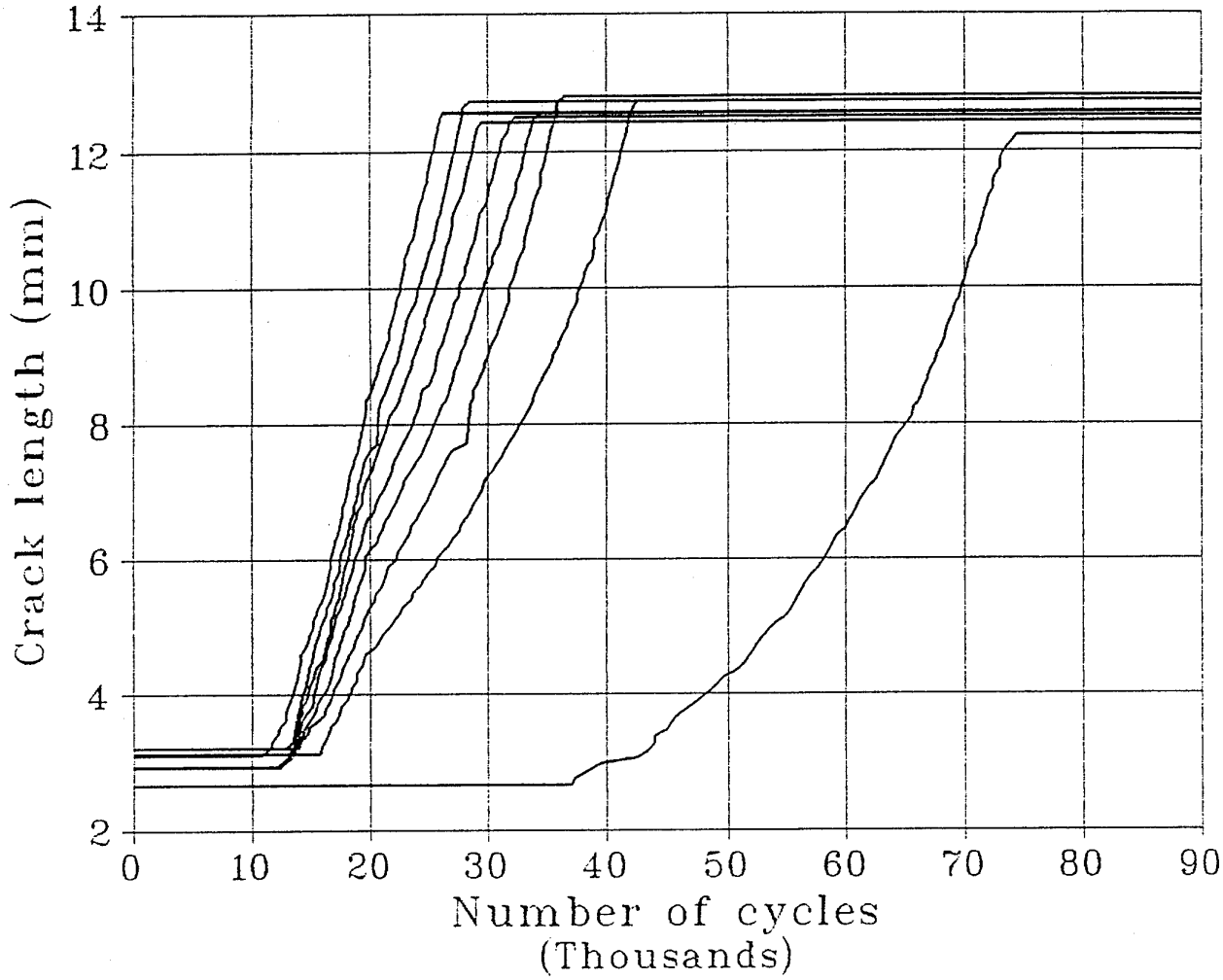

Fig. 13. Crack growth plot for the specimen No. 1

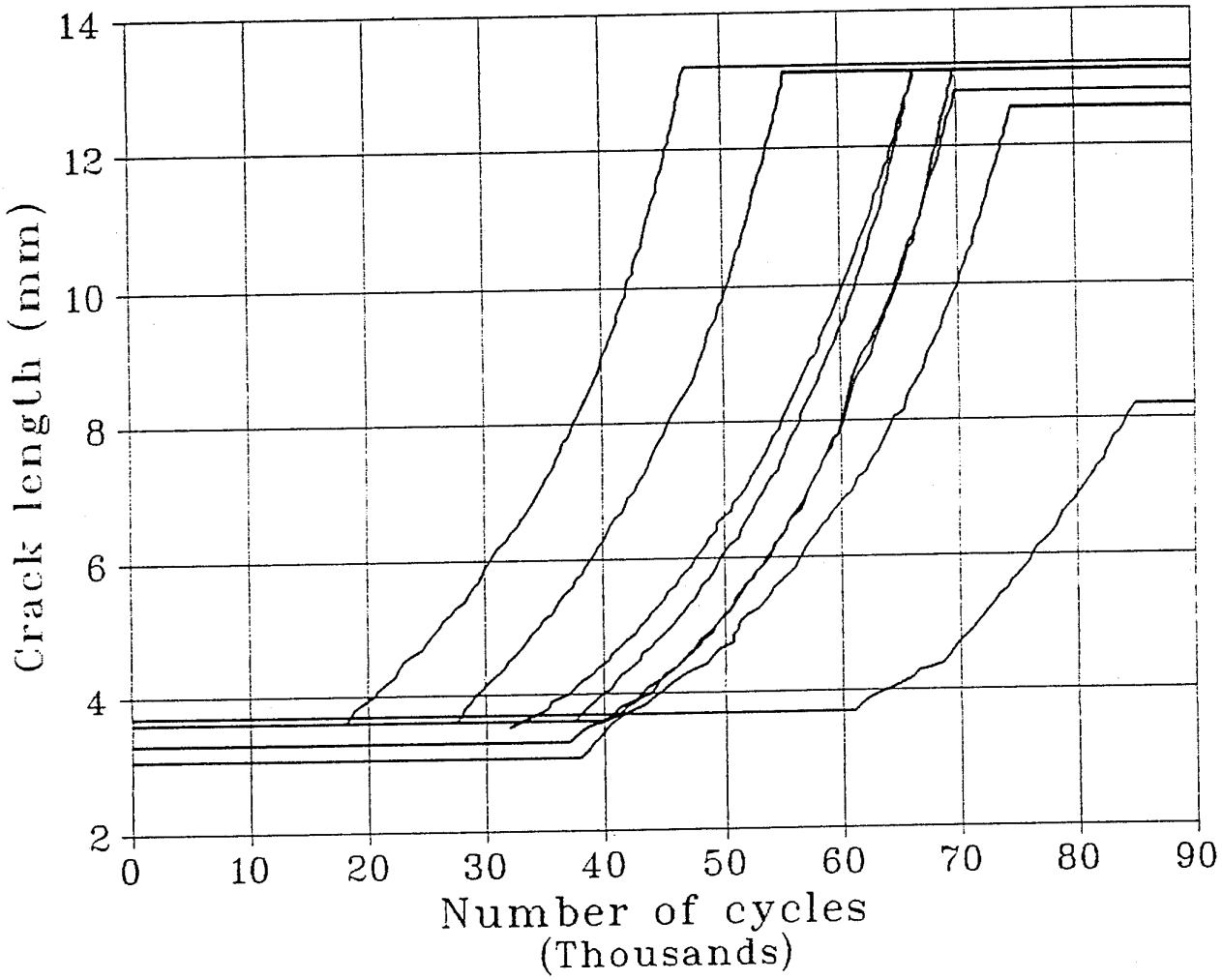

Fig. 14. Crack growth plot for the specimen No. 2

As can be seen from the above plots the coordinates of the initial (and the final) points of the crack propagation curves differ one from each other. The vertical scatter of the initial points is due to differences in locations of the first strand of the crack propagation gauges. The horizontal scatter of the initial points is due to statistical scatter of the crack initiation time. The scatter of the crack length is enhanced in the course of fatigue crack growth due to the stochastic nature of the crack propagation process. Scatter of the crack lengths caused definite problems since some cracks could run off and become long enough to influence the growth of the other cracks. To avoid such situations, all the cracks just crossing the final strand of the second crack propagation gauge were drilled at crack tip by a drill of 5 mm, as can be seen from Fig. 15. By this means further crack propagation was prevented.

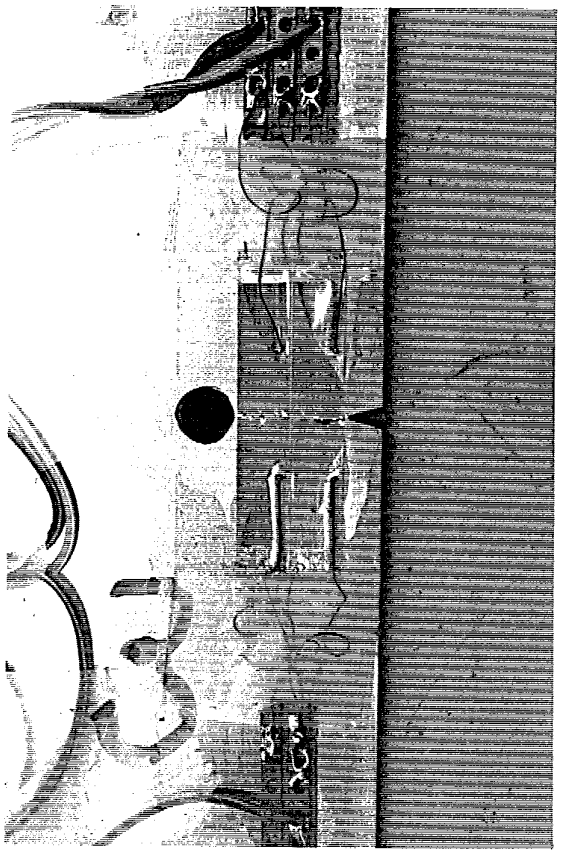

Fig. 15 Close up showing fatigue crack drilled at its tip after crossing two crack propagation gauges

Further analysis of the experimental data is based on an assumption that during each loading cycle the crack extends in accordance with power law (Paris law):

$$\frac{da}{dN} = C\cdot(\Delta K)^m \qquad (7)$$

with C being random characteristic of material field and m being a constant value. Here ΔK is the stress intensity factor range determined by the stress range, $\Delta\sigma = \sigma_{max} - \sigma_{min}$, and crack length, a, as follows:

$$\Delta K = 1.12\cdot Y(a)\cdot\Delta\sigma\cdot\sqrt{\pi a}\ , \qquad (8)$$

where Y(a) is a geometrical factor close to 1 for the short cracks.

First of all for each crack in the array the average coefficient C_i, characteristic of the crack under consideration, and the exponent m_i were determined by application of linear regression procedure to the experimental data given in logarithmic coordinates $\ell n \frac{da}{dN}$ versus $\ell n\Delta K$ (see equation (7)).

Here $\frac{da}{dN}$ was determined using constant value of crack increment predetermined by the interstrand spacing of the crack propagation gauge (da = 0.1mm) and the number of cycles corresponding to each crack increment; the latter is a variable value. Since the $\frac{da}{dN}$ values are characterized by significant scatter coefficient of correlation between $\ell n \frac{da}{dN}$ and $\ell n\Delta K$ proved to be somewhat low (about 0.7).

To circumvent this difficulty an integral method of C_i and m_i determination was applied. Integrating equation (7) and having in mind (8), the following expression can be obtained.

$$N-N_{o_i} = \frac{2}{C_i(1.12\cdot\Delta\sigma\sqrt{\pi})^{m_i}\cdot(m_i-2)}\left[\frac{1}{a_0^{\frac{m_i-2}{2}}} - \frac{1}{a^{\frac{m_i-2}{2}}}\right] \qquad (9)$$

where a_0 – initial crack length

N_{o_i} – number of cycles corresponding to the onset of crack growth.

For instance a crack length corresponding to the position of the first strand in the first crack propagation gauge can be adopted as a_0 value. N_{o_i} in this case is

number of cycles preceding the cutting of the first strand by the crack. Nevertheless, it seems reasonable to assume that a_0 equals to the prenotch (crack starter) depth. N_{o_i} in this case cannot be obtained directly from experimental data and should be considered as a parameter to be determined. Algorithm of C_i, m_i, and N_{o_i} determination was as follows:

1. An initial value of m_i is selected.
2. Linear regression between the random experimental values N_j and $\left[\frac{1}{a_0^{\frac{m_i-2}{2}}} - \frac{1}{a^{\frac{m_i-2}{2}}}\right]$ is established and N_{o_i} is determined as free term of the regression and $\frac{1}{C_i}$ – as its tangent coefficient.
3. The measure of "incompatibility" is computed as sum of squares of the deviations of the experimental values N_j from the corresponding values deduced from the linear regression expression $N(a_j)$:

$$\delta = \sum_j (N(a_j) - N_j)^2 \qquad (10)$$

4. The new value of m_i is selected and the procedure is repeated.
5. The above procedure was repeated several times until minimal δ value is found.

Another option of above procedure is based on the simultaneous consideration of all the cracks under condition that the value of parameter m is common to all the cracks. In this case the individual values of C_i for each crack were determined using the same value of m. The measure of "incompatibility" in this case is as follows:

$$\delta = \sum_i \sum_j (N_i(a_j) - N_{ij}) \qquad (11)$$

where N_{ij} corresponds to experimental results and $N_i(a_j)$ to linear regression expression, i corresponds to the crack number and j to the crack propagation step number (gauges strand number).

It should be noted that the correlation coefficients characteristics of the above integral method are above 0.98. The values of C_i, m_i and m deduced from the experimental results of the specimens No. 1 and No. 2 are presented in Table 4.

Table 4. Parameters of power law deduced from CA-loading test results (specimens No. 1 and No. 2)

Specimen No.	Parameters	Crack Nos. 1	2	3	4	5	6	7	8
1	Individual exponent, m_i	2.42	1.94	2.17	2.62	2.31	1.48	2.54	2.47
	$C_i \cdot 10^9$	2.30	6.40	4.22	1.44	2.68	22.7	1.44	1.70
	$N_{o_i}(a_0=2.5mm)$	-2734	2148	-792	1024	-327	4890	1425	34801
	Global exponent, m	2.47	2.47	2.47	2.47	2.47	2.47	2.47	2.47
	$C_i \cdot 10^9$	2.05	1.96	2.13	2.00	1.88	2.33	1.66	1.70
2	Individual exponent, m_i	2.46	2.52	2.64	2.71	2.43	2.53	2.55	2.99
	$C_i \cdot 10^9$	1.61	1.54	1.22	1.07	1.92	1.33	1.48	0.516
	$N_{o_i}(a_0=3.0mm)$	28566	12771	35352	35460	22107	36250	32405	54074
	Global exponent, m	2.56	2.56	2.56	2.56	2.56	2.56	2.56	2.56
	$C_i \cdot 10^9$	1.30	1.41	1.44	1.46	1.46	1.25	1.45	1.21

Note: The C_i values correspond to the stresses in MPa and crack lengths in m.

It should be noted that negative values of N_{o_i} obtained for some cracks belonging to the specimen No. 1 are due to forced crack growth conditions on the initial stages of the process (up to 20000 cycles) whereas the calculations were performed using final conditions established after 20000 cycles.

Data of the Table 4 shows that the exponent m_i exhibits much lower scatter than the coefficient C_i. Thus in the case of the specimen No. 1* the m_i values are confined by the range 1.94 - 2.62, i.e., the maximum change is about 1.35 times, whereas the corresponding values of the coefficient C_i are in the range from

*Crack No. 6 was excluded from consideration.

$1.44 \cdot 10^{-9}$ to $6.4 \cdot 10^{-9}$, i.e., 4.44 times. In the case of specimen No. 2 the scatter is even smaller: the maximum change of m_i is 1.23 and of C_i - 3.72.

In the case of application of the common value of the exponent m (global m), the optimal values found for both specimens are quite close: 2.47 in the case of the specimen No. 1 and 2.56 in the case of the specimen No. 2. Using the calculated values of N_{o_i}, C_i and m_i the regression curves of crack growth were "reduced" to a common initial point:

a_0 = 2.5 mm and N_0 = 0 in the case of the specimen No. 1, and

a_0 = 3mm and N = 0 in the case of the specimen No. 2.

Figs. 16 and 17 show corresponding experimental crack growth curves located in accordance with their regression curves.

As can be seen from the above figures the crack growth exhibits stochastic behaviour being locally irregular along the crack curve and displaying significant scatter of these curves. The latter diverge more and more as cracks grow, and a weak mixing can be observed (see Fig. 17). In spite of the significant divergence of the crack curves, the ratio of the maximal to the minimal life time, N_{max}/N_{min} for different crack lengths remains almost constant: about 2 in the case of the specimen No. 1, and about 1.3 in the case of the specimen No. 2.

More detailed probabilistic analysis of the experimental results is planned to perform in continuation of the research with development of stochastic model describing the multiple crack growth in a random medium.

4.2 Fatigue crack behaviour under CA loading with superimposed overload peaks

It is well known that stepwise change of the cycle amplitude can lead to a deviation of the crack growth rate from the crack growth power law [7-11]. Transition to a level with higher stress intensity factor, K_{max}, causes temporary increase of the crack growth rate with respect to that expected in accordance with the power law.

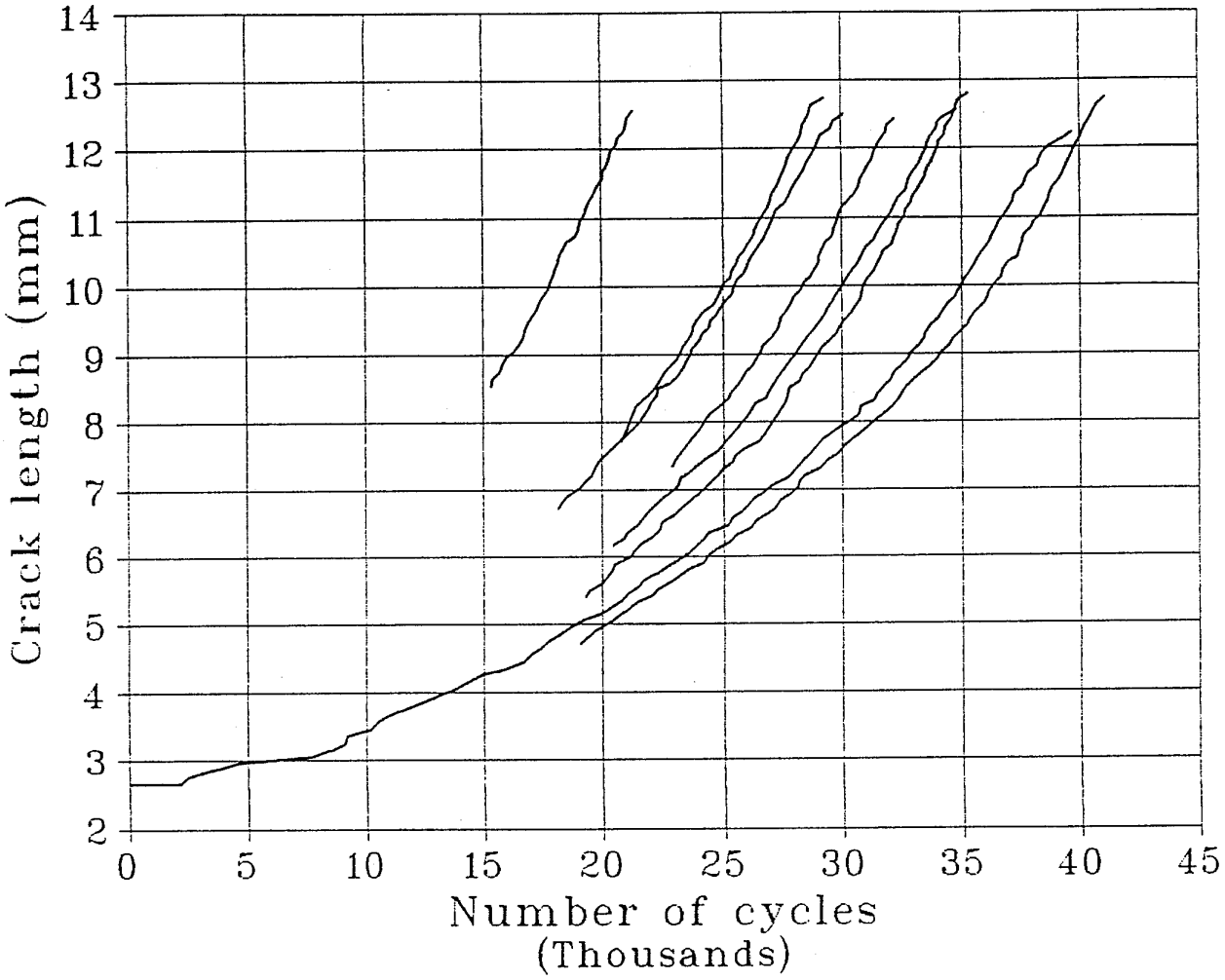

Fig. 16. Crack growth curves of the specimen No. 1 reduced (via their regression curves) to the common initial point (a_0=2.5mm, N_{o_i}=0)

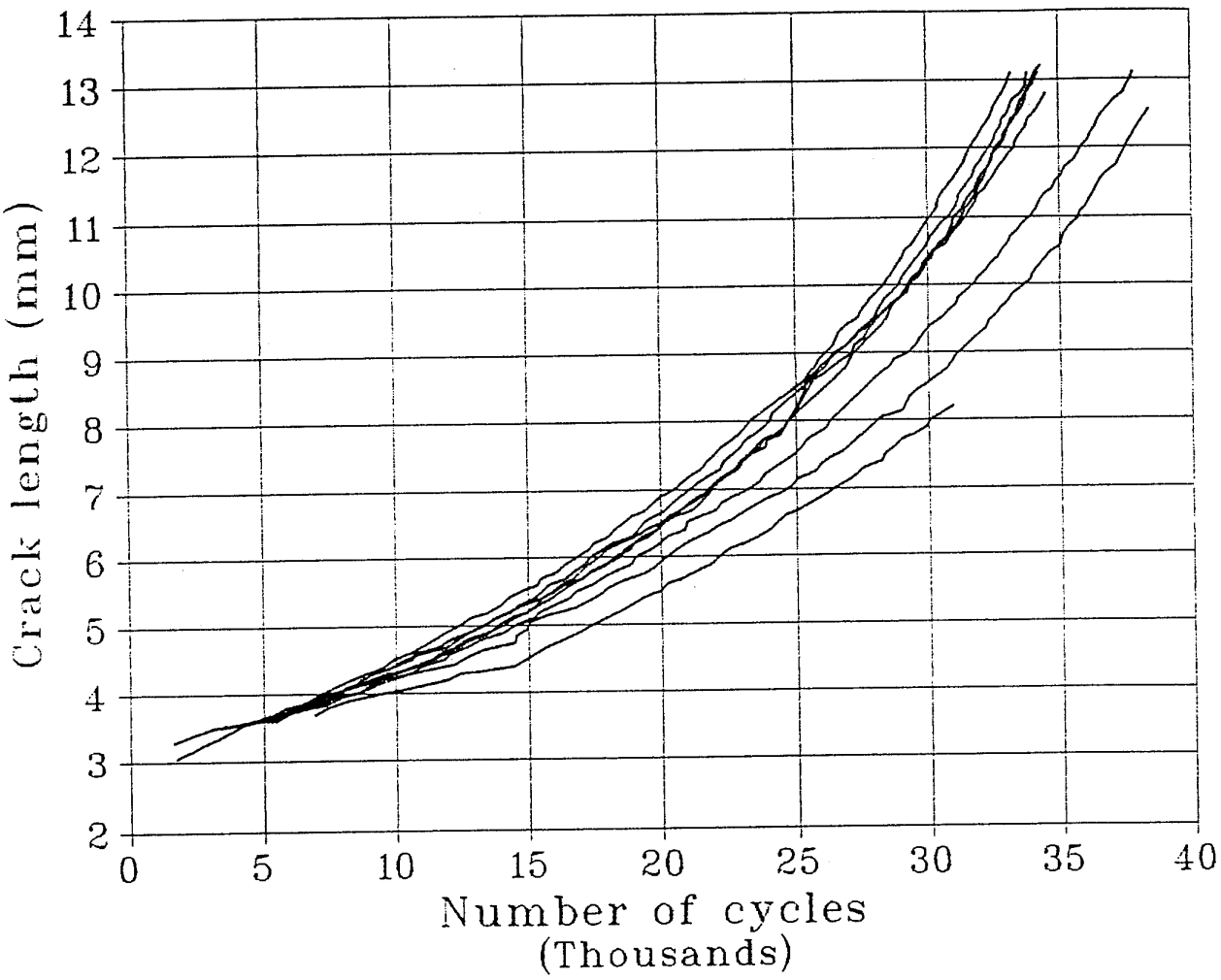

Fig. 17. Crack growth curves of the specimen No. 2 reduced (via their regression curves) to the common initial point (a_0=3mm, N_{o_i}=0)

On the contrary decrease of K_{max} can cause a temporary reduction in the crack growth rate (retardation effect) and even — a full arrest of crack growth. The retardation effect is associated with local plastic deformation at crack tip causing crack closure effect [12-17]. In the present work single peak overloads were used for investigation of the retardation effect.

The multicrack specimen (No. 3) was tested under the following parameters of CA-loading: P_{max} = 39200N, P_{min} = 19600N corresponding to the following nominal cycle stresses: σ_{max} = 98MPa, σ_{min} = 49MPa. From time to time single overload peaks were superimposed on CA-loading causing temporary arrest of the cracks. The overload ratio was determined in the terms of the stress intensity factors (SIF's) of basic and overload cycles, as follows:

$$R_{OVL} = \frac{K_{0max} - K_{min}}{K_{max} - K_{min}}$$

where K_{0max} - is the SIF corresponding to the overload peak and K_{max} and K_{min} are maximum and minimum SIF's of the base-line CA-loading respectively.

After each overload the base-line CA-loading was kept unchanged until all the cracks recommmenced to grow with the rate as before the overload. The following values of R_{OVL} were applied in this study: 1.25; 1.5; 1.75; 2.0; 2.25; 2.5. Fig. 18 exhibits the crack growth curves of specimen No. 3, tested with application of above overloads. The number of the overloads fallen upon each individual crack was different. One of the cracks escaped the overloads at all, being initiated and finished during the long arrest of the other cracks after a strong overload (R_{OVL}=2.5). Analysis of the obtained data showed that the crack growth delay time depends on both the overload intensity and the crack length. Table 4 shows the delay time values corresponding to the different crack lengths and overload ratios. Fig. 19 shows delay time dependence on the overload ratio. Significant scatter of the experimental points corresponding to the same overload ratio is due to the different crack lengths.

Table 4. Results of delay time determination for cracks of the specimen No. 3

Overload No.		1	2	3	4	5	6	7	8	9
Overload ratio K_{OVL}		1.25	1.5	1.75	2.0	2.25	2.5	1.75	2.0	2.25
Time of the over-load application (number of cycles)		26003	29009	32009	35009	40005	50011	95003	97647	104004
Crack No. 1	crack length, mm		3.75	4.45	5.15	6.25	8.15			
	delay time		500	1500	2750	6500	29200			
Crack No. 2	crack length, mm	3.65	4.55	5.65	5.65	6.55	7.85	8.3		
	delay time	750	700	1000	1000	2750	10000	23500		
Crack No. 3	crack length, mm			4.0	4.5	5.2	7.2	9.0	9.6	11.2
	delay time			500	2800	6000	40000	1800	2400	13000
Crack No. 4	crack length, mm		4.1	4.6	5.1	5.9	6.7			
	delay time		1000	1100	2700	8200	25200			
Crack No. 5*	crack length, mm									
	delay time									
Crack No. 6	crack length, mm	3.7	4.5	5.1	6.1	7.2	8.1	10.7	12.1	12.2
	delay time	500	750	600	2550	7500	43000	1500	6200	14300
Crack No. 7**	crack length, mm									
	delay time									
Crack No. 8	crack length, mm			3.8	4.2	4.6	5.8			
	delay time			1250	4000	7100	22500			

* The crack No. 5 did not initiate during the test time.

** The crack No. 7 is initiated and finished during the time of the crack arrest caused by application of the strong overload (K_{OVL} = 2.5)

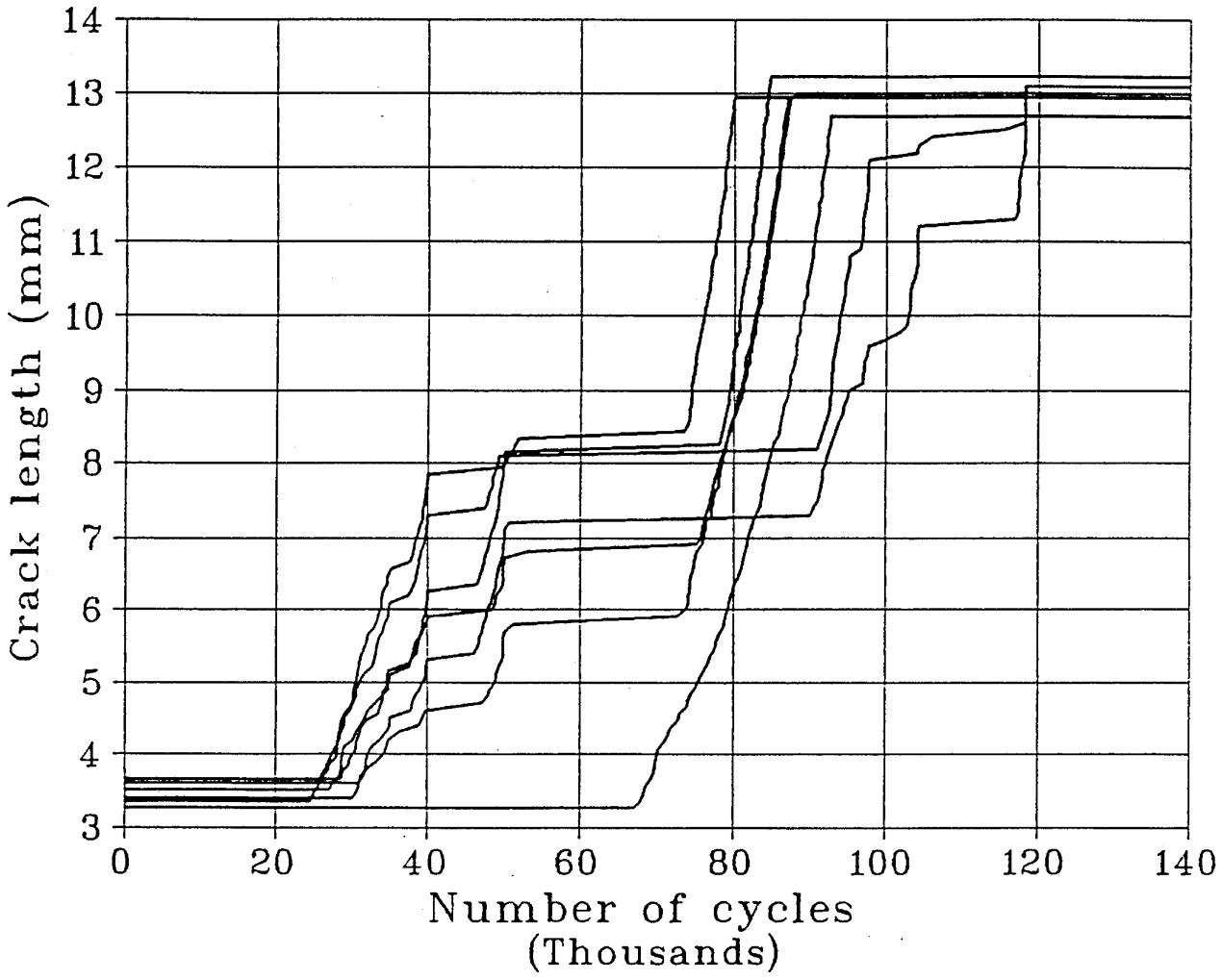

Fig. 18. Crack growth curves corresponding to the CA-loading with superimposed overloads (specimen No. 3). Note horizontal segments of the curves corresponding to after-overload delay times.

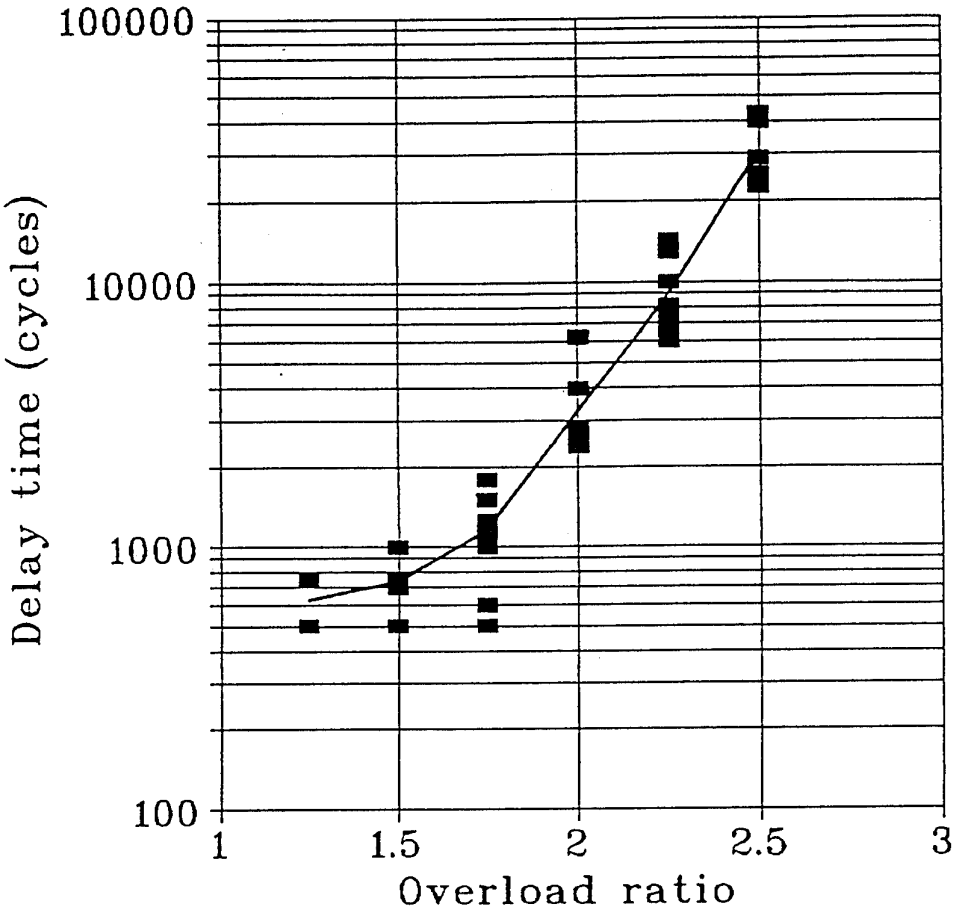

Fig. 19. Plot of the delay time as a function of the overload ratio.

Figs. 20 and 21 show the dependence of the delay time on the crack length for the overload factors 2.25 and 2.5 respectively. As can be seen from the above figures there is a strong tendency to delay time increase with the increase of crack length (about two times). Nevertheless the limited amount of data and their significant scatter do not permit presentation of the above dependence in a more explicit form.

4.3. Crack growth under random loading (RL)

In Chapter 3.2 the procedure of computer generation of a stationary Gaussian process with average zero, standard deviation unity and a correlation function given by equation (6) was described. After elimination of the ranges smaller than two standard deviations (presumably not influencing crack growth), the transition frequencies from peaks to troughs and vice versa were presented in the form of the two-dimensional matrix (Table 1). This matrix was the basis for the real-time generation of a random sequence of the reversals corresponding to the normalized random process with a given autocorrelation function (6). Using linear transform the above sequence of reversals was transformed into reversal sequence corresponding to the random process with mean value and standard deviation required for a test in question.

The following table shows the loading parameters applied in the course of the random loading tests.

Table 5. Loading Parameters of RL Tests

Specimen No.	Mean Load, P_{mean}, N	Standard Deviation of the Loading Process, Std, N	Elimination Threshold
4	29400	4900	1 Std
5	29400	4900	2 Std
6	34300	4900	2 Std
7	24500	4900	2 Std
8	29400	3920	2 Std
9	29400	5880	2 Std

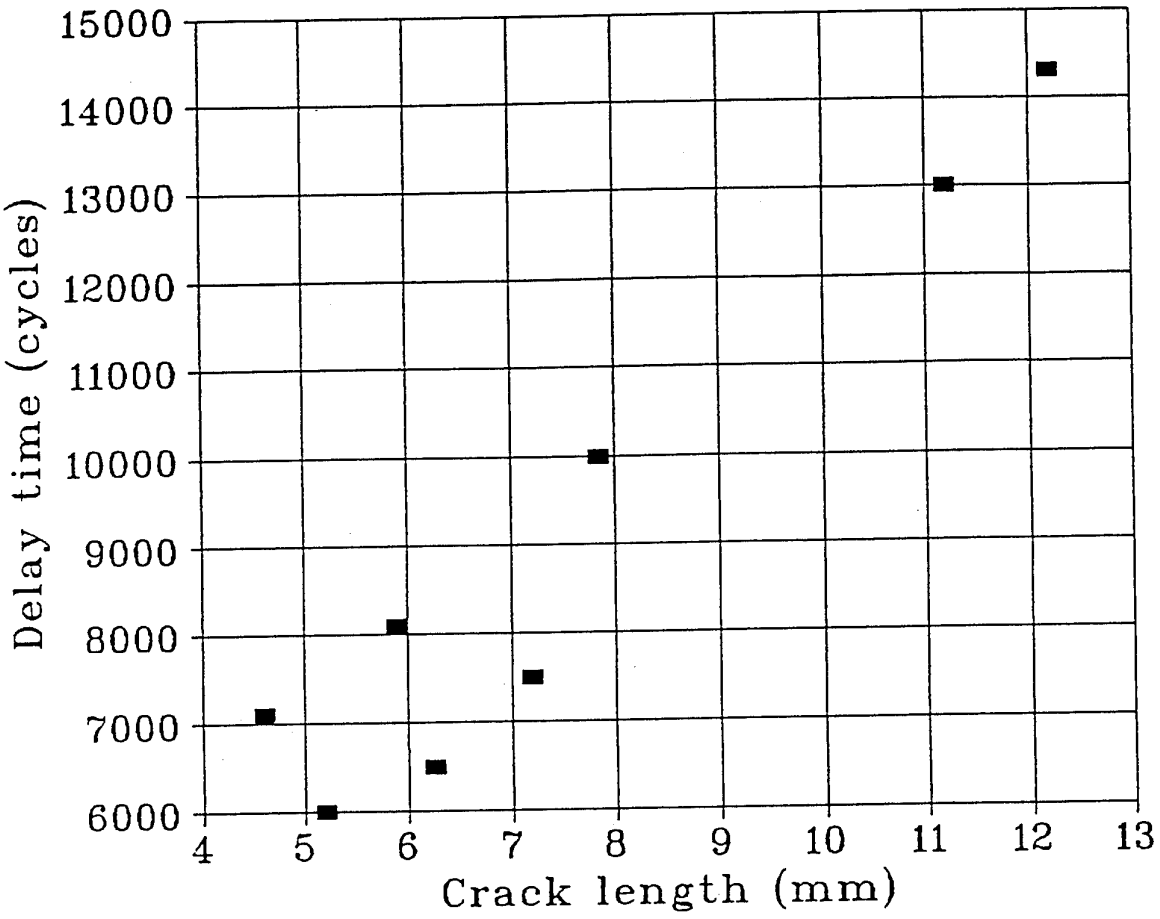

Fig. 20. Delay time as a function of the crack length.
Overload ratio R= 2.25

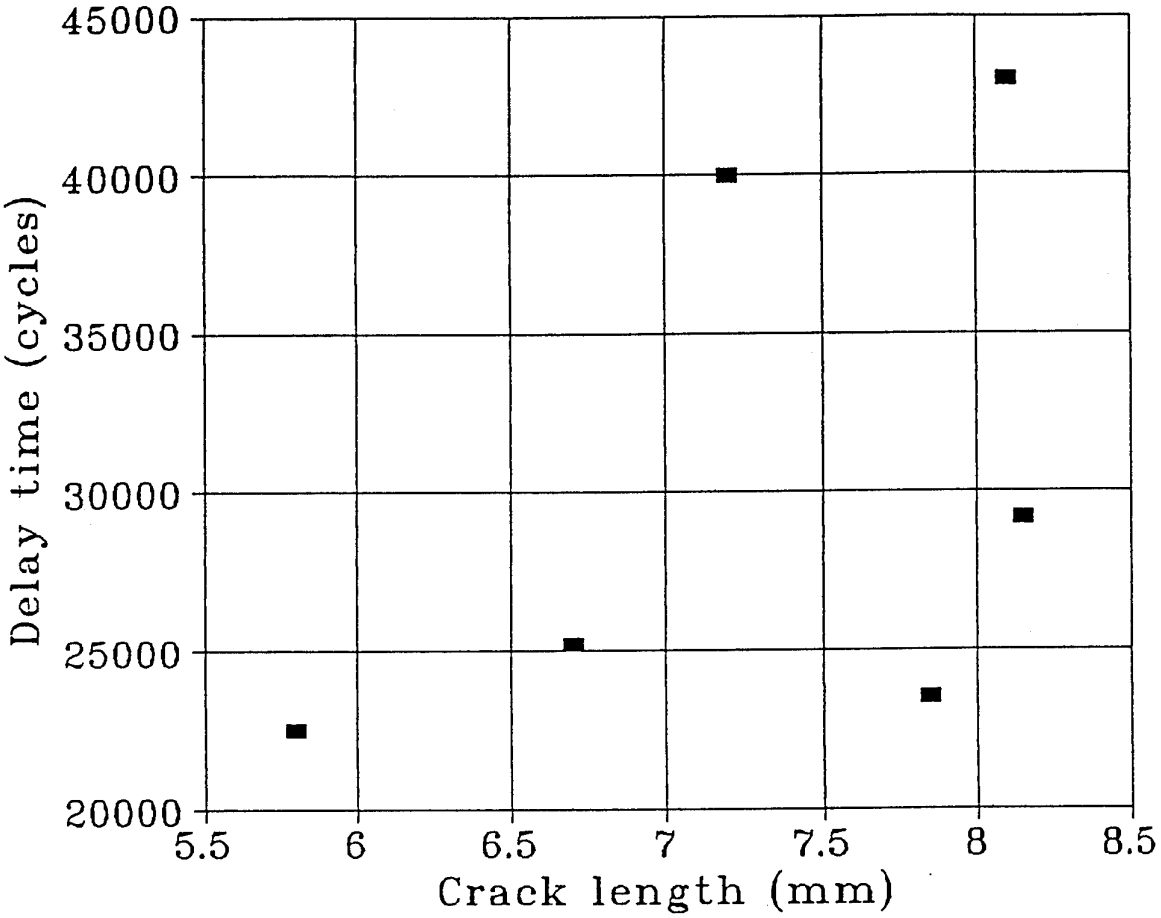

Fig. 21. Delay time as a function of the crack length.
Overload ratio R = 2.5.

Thus, both the mean load and the standard deviation have been varied during the tests. As can be seen from Table 5 the elimination level in the case of the specimen No. 4 is twice lower than in all the other specimens. This was done for verification of the elimination threshold. Analysis of the transition matrix used in the test of the specimens No. 4 and that of No. 5 showed that the number of ranges confined within the interval from 1 Std to 2 Std is about a half the number of all the ranges greater than one standard deviation. Since the life time of the cracks belonging to the specimen No. 4 proved to be almost exactly twice longer than in the specimen No. 5. it can be concluded that the ranges smaller than two standard deviations almost do not contribute to the crack growth in the case of the loading conditions used in these tests. Since the loading conditions envisaged for the other specimens have to be varied within relatively narrow limits it was assumed that the elimination of small ranges using the threshold equal to two standard deviations would not influence the crack growth. Figs. 22 to 26 exhibit crack growth curves for all above mentioned types of random loading.

These curves have been reduced to a common initial crack length (equal to 3 mm) by the procedure described in Chapter 4.1. For application of this procedure the stress range $\Delta\sigma$ in regression equation was assumed to be equal to six standard deviations (reference range). Exactly as in the case of CA-loading also in the RL-loading the parameters N_{0_i}, m_i, C_i were determined for each individual crack. These parameters are presented in Table 6. The crack growth curves reduced to the common origin are shown in the Figs. 27-31. The values of parameter C_i are of conditional character since they are dependent on the accepted reference range, whereas (as can be shown) N_{o_i} and m_i are invariant relative to the value of the reference range. The C_i values presented in the Table 6 are computed using the 6 Std. reference range value. From analysis of the crack life time curves (Figs. 27-31) it can be concluded that the maximal-to-minimal life time ratio is almost independent of the crack length and equals to 1.3-1.4. These figures are similar to those obtained in the case of CA loading (specimen No. 2.).

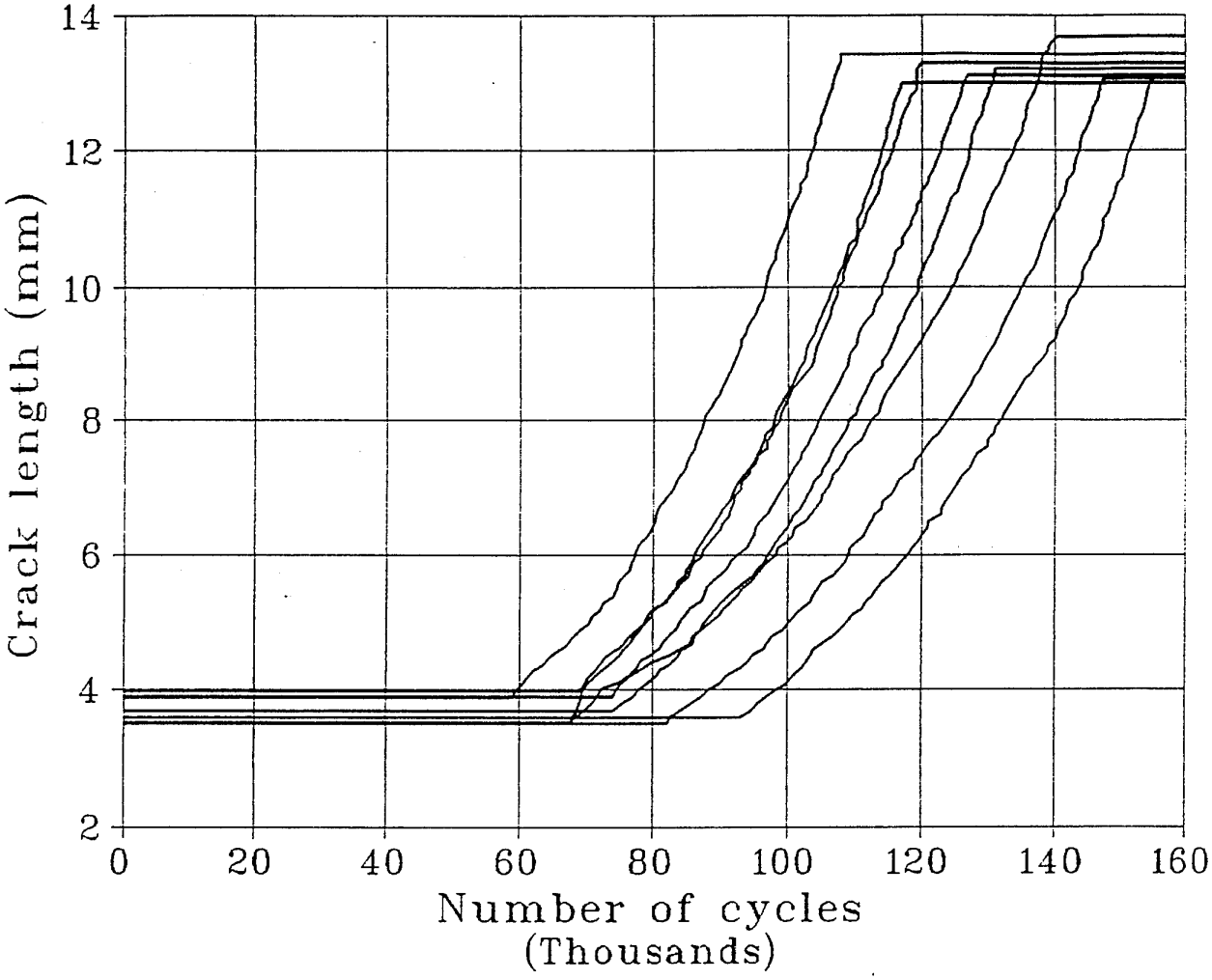

Fig. 22. Dependence of the crack length on the number of cycles. Specimen No. 5.

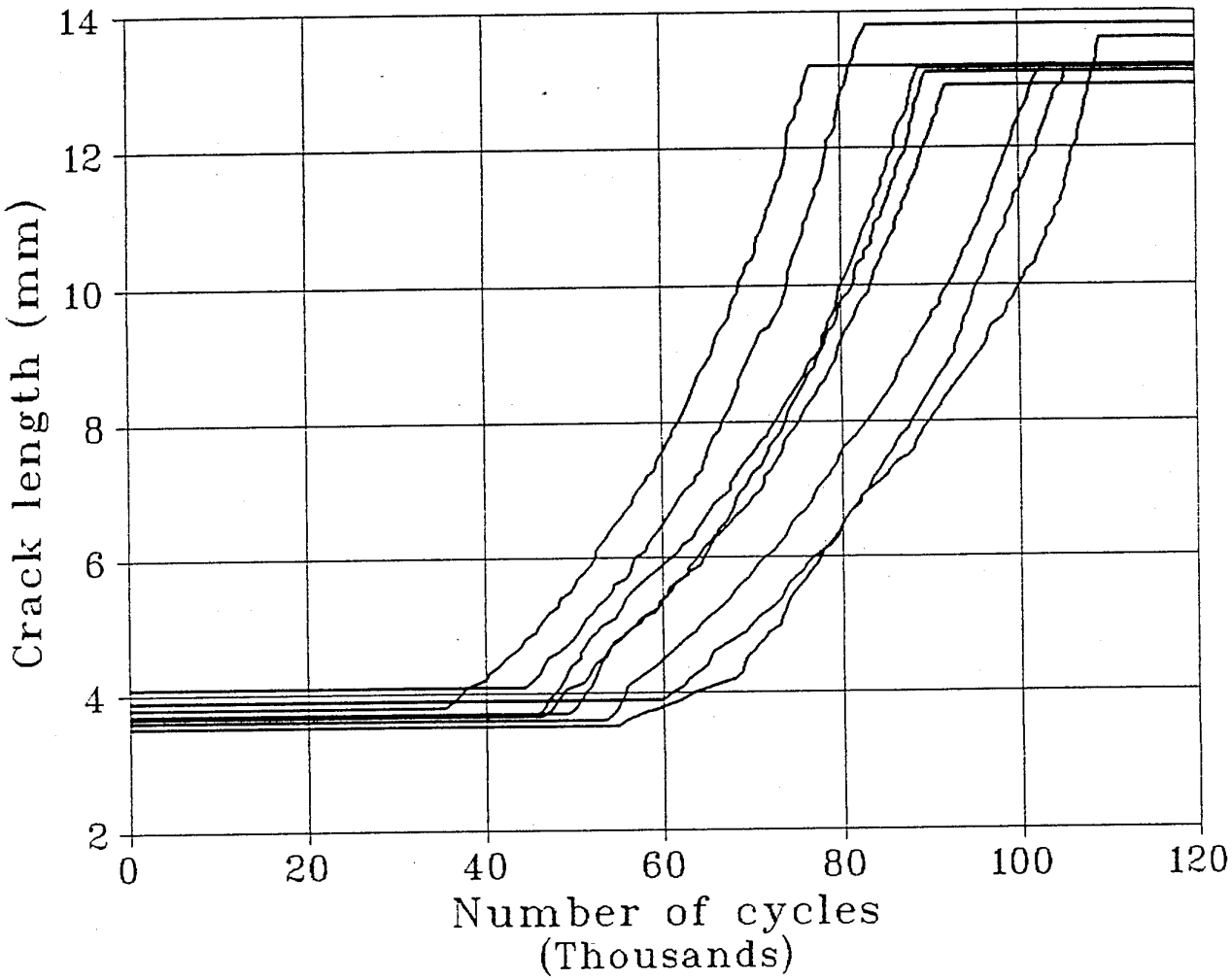

Fig. 23. Dependence of the crack length on the number of cycles. Specimen No. 6.

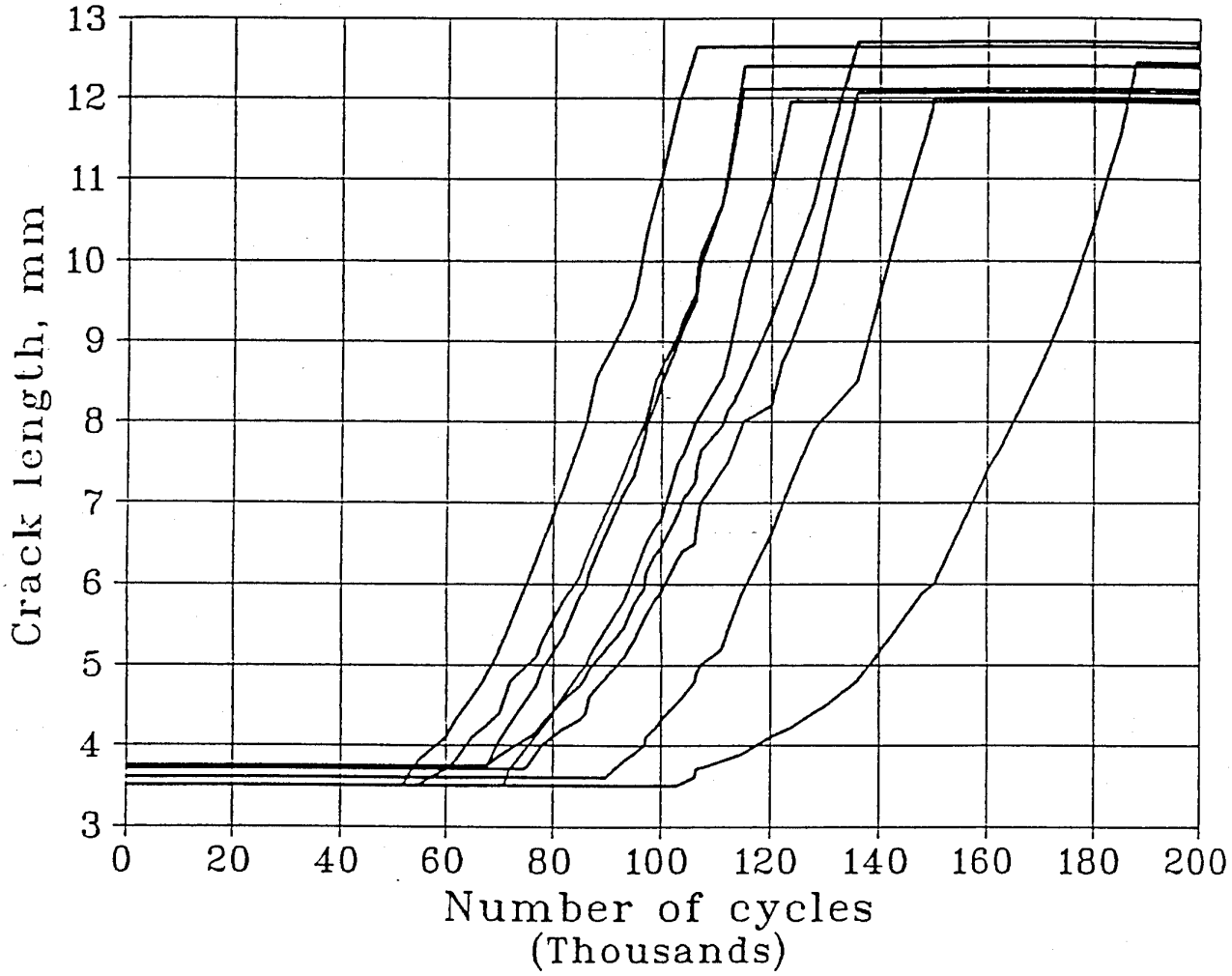

Fig. 24. Dependence of the crack length on the number of cycles. Specimen No. 7.

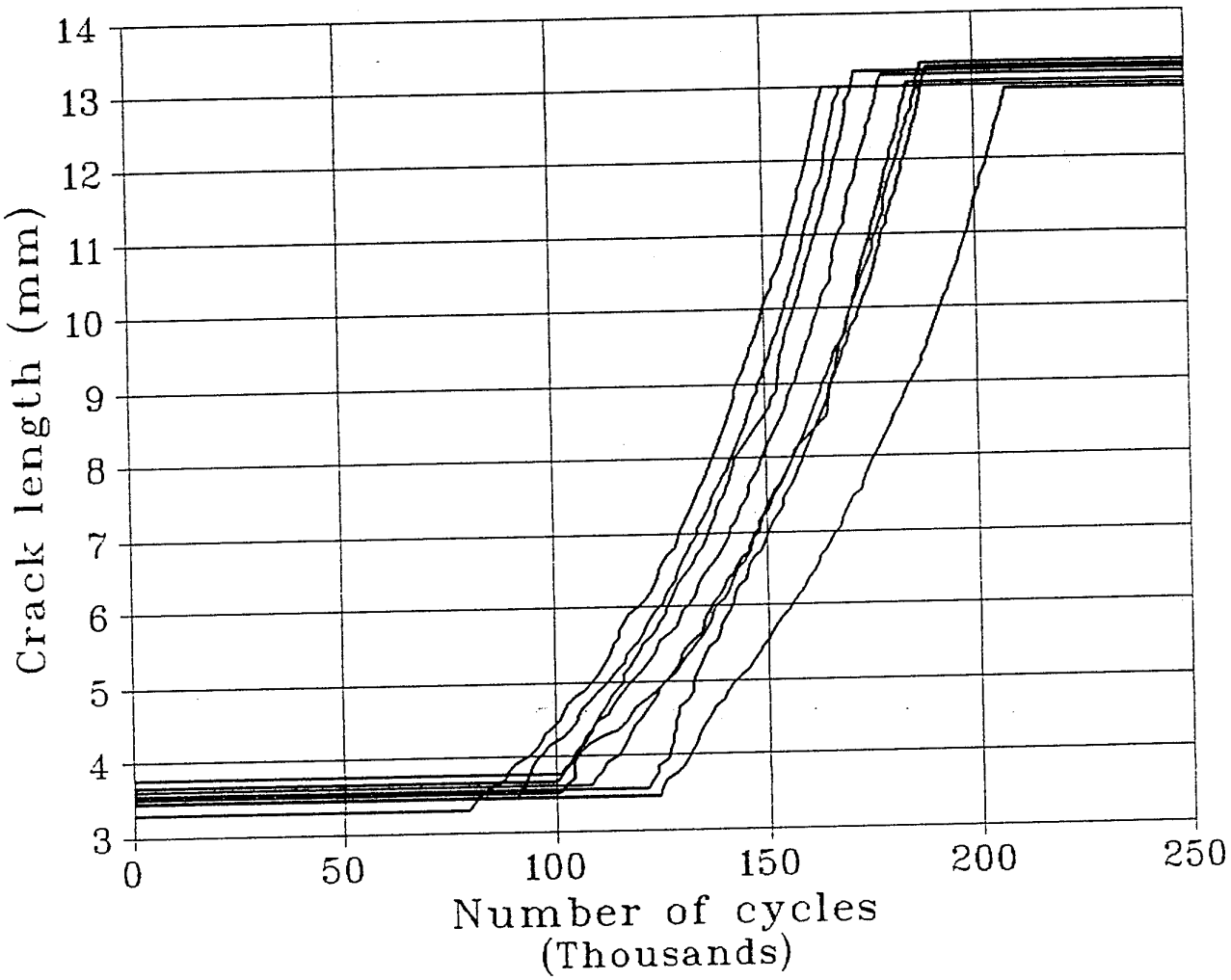

Fig. 25. Dependence of the crack length on the number of cycles. Specimen No. 8.

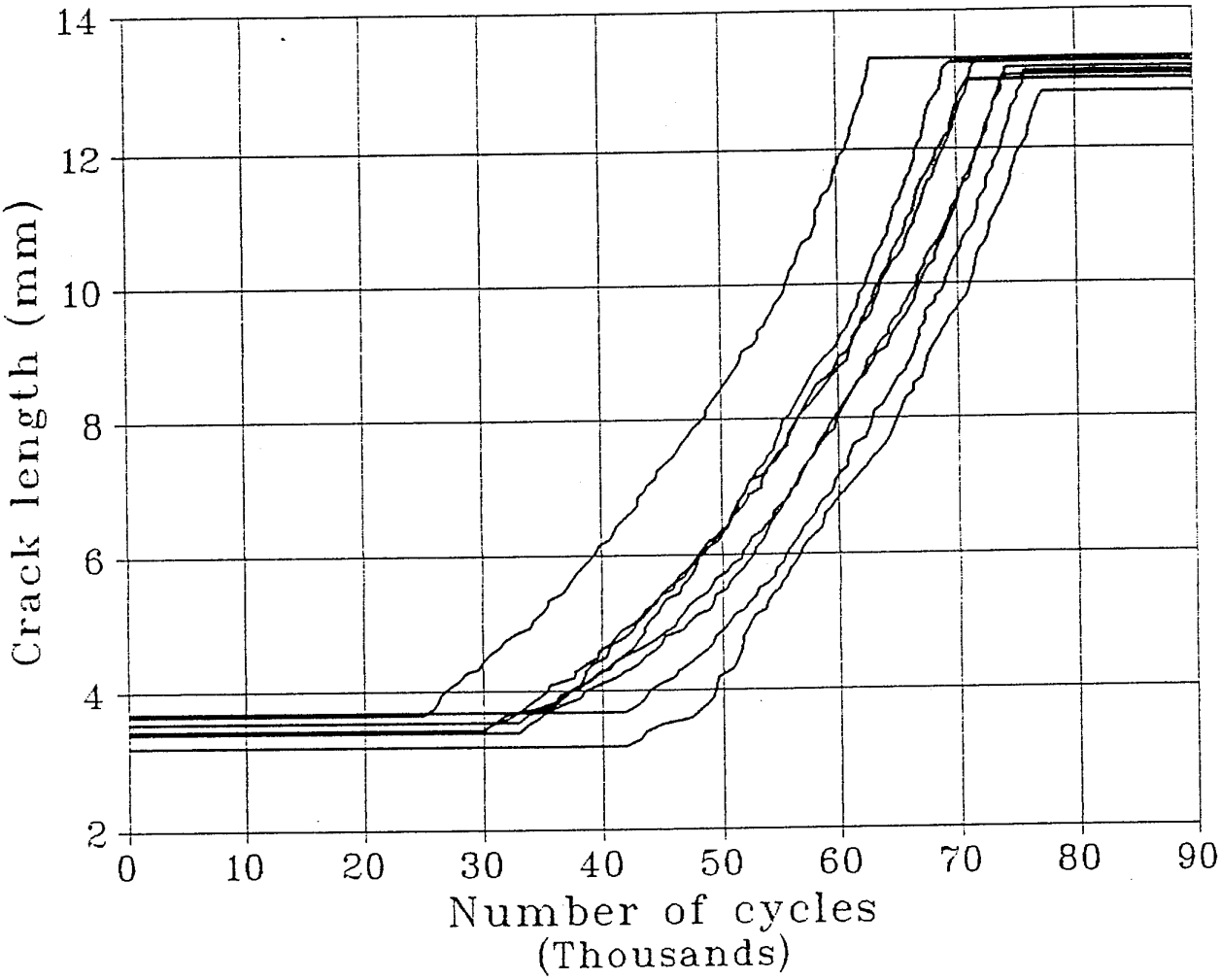

Fig. 26. Dependence of the crack length on the number of cycles. Specimen No. 9.

Table 6. Parameters of exponential law applied to RL crack growth

Specimen No.	Parameters	Crack Nos. 1	2	3	4	5	6	7	8
No. 5	Individual exponent, m_i	2.16	1.97	2.17	2.09	2.31	2.09	2.26	2.14
	$C_i \cdot 10^9$	3.52	4.95	3.03	3.27	2.02	3.17	2.77	3.28
	$N_{Oi}(a_0=3.0mm)$	49085	59255	64706	84089	58865	71149	55890	60742
P_{mean} = 28400N Std = 4900N	Global exponent, m	2.15	2.15	2.15	2.15	2.15	2.15	2.15	2.15
	$C_i \cdot 10^9$	3.66	3.57	3.20	2.93	2.72	2.84	3.40	3.22
No. 6	Individual exponent, m_i	1.94	1.83	2.52	2.11	2.18	2.51	2.54	2.25
	$C_i \cdot 10^9$	5.82	6.50	2.82	4.25	3.85	2.26	2.18	3.46
	N_{0_i}	40121	45406	46574	35700	53540	26398	31846	38319
P_{mean} = 34300N Std = 4900N	Global exponent, m	2.16	2.16	2.16	2.16	2.16	2.16	2.16	2.16
	$C_i \cdot 10^9$	3.90	3.56	3.33	3.88	4.00	4.30	4.43	4.08
No. 7	Individual exponent, m_i	2.07	2.07	1.92	2.04	2.33	2.27	2.17	2.12
	$C_i \cdot 10^9$	3.76	4.09	5.39	3.60	2.17	2.11	2.61	2.81
	N_{0_i}	63186	46181	58535	82066	48725	108599	57778	63448
P_{mean} = 24500N Std = 4900N	Global exponent, m	2.12	2.12	2.12	2.12	2.12	2.12	2.12	2.12
	$C_i \cdot 10^9$	3.38	361	3.63	3.02	3.14	2.71	2.76	2.81
No. 8	Individual exponent, m_i	1.77	2.25	1.03	2.46	1.74	2.37	2.37	2.59
	$C_i \cdot 10^9$	7.36	3.21	2.55	2.30	6.63	2.67	2.58	1.70
	N_{0_i}	88601	93643	93844	71853	112777	83011	77750	82826
P_{mean} = 294600N Std = 3920N	Global exponent, m	2.20	2.10	2.10	2.10	2.10	2.10	2.10	2.10
	$C_i \cdot 10^9$	4.30	4.08	4.53	4.06	3.73	3.98	4.10	3.74
No. 9	Individual exponent, m_i	2.04	1.90	2.23	2.75	2.43	1.39	2.16	2.12
	$C_i \cdot 10^9$	3.91	5.47	2.69	0.93	1.88	17.6	3.55	3.86
	N_{0_i}	18024	28816	25828	25309	29325	42465	29371	36555
P_{mean} = 29400N Std = 5880N	Global exponent, m	2.16	2.16	2.16	2.16	2.16	2.16	2.16	2.16
	$C_i \cdot 10^9$	3.07	3.24	3.09	3.01	3.24	3.81	3.56	3.56

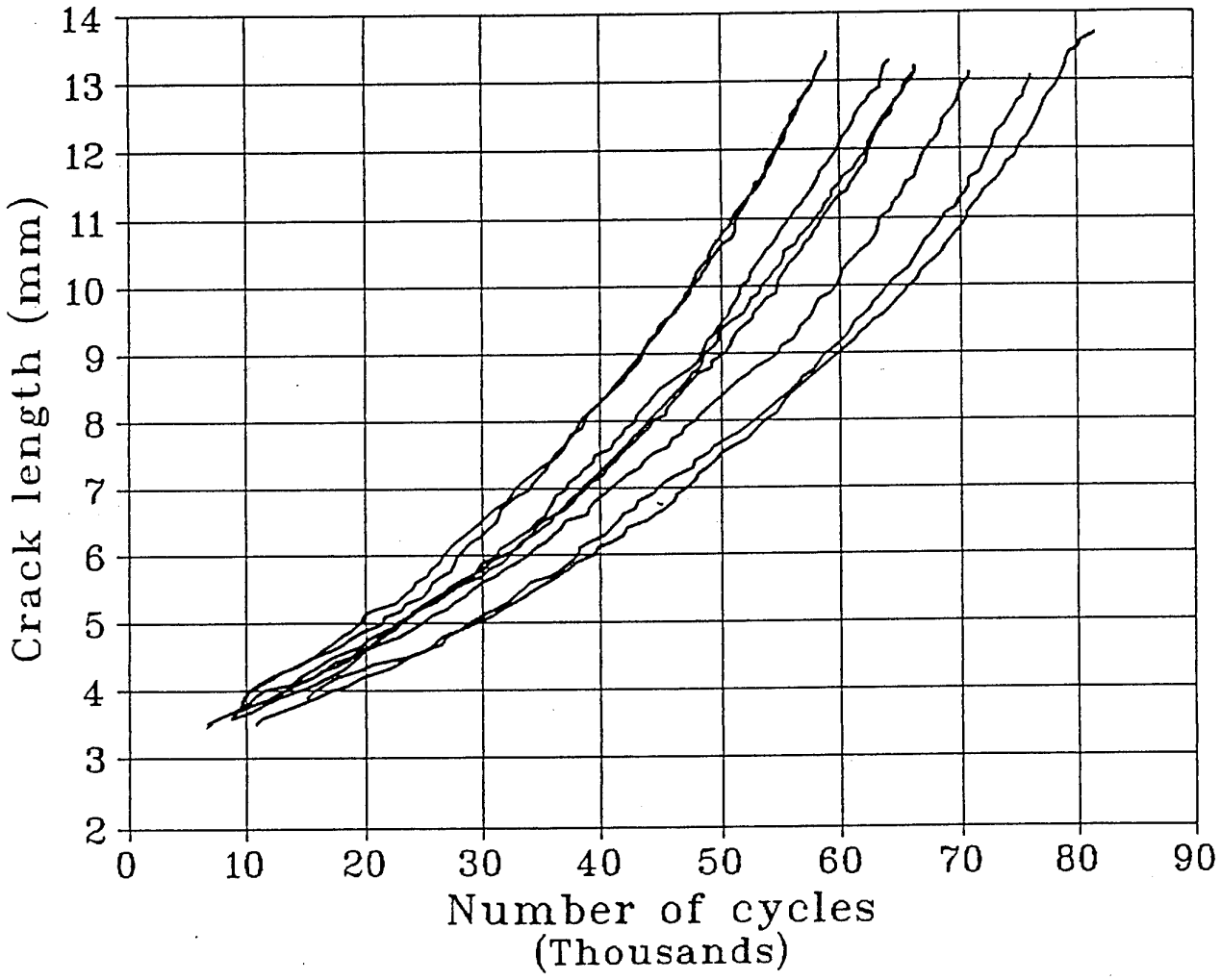

Fig. 27. Crack growth curves of the specimen No. 5 reduced via their regression curves to the common initial point (a_0=3mm, N_{0_i}=0)

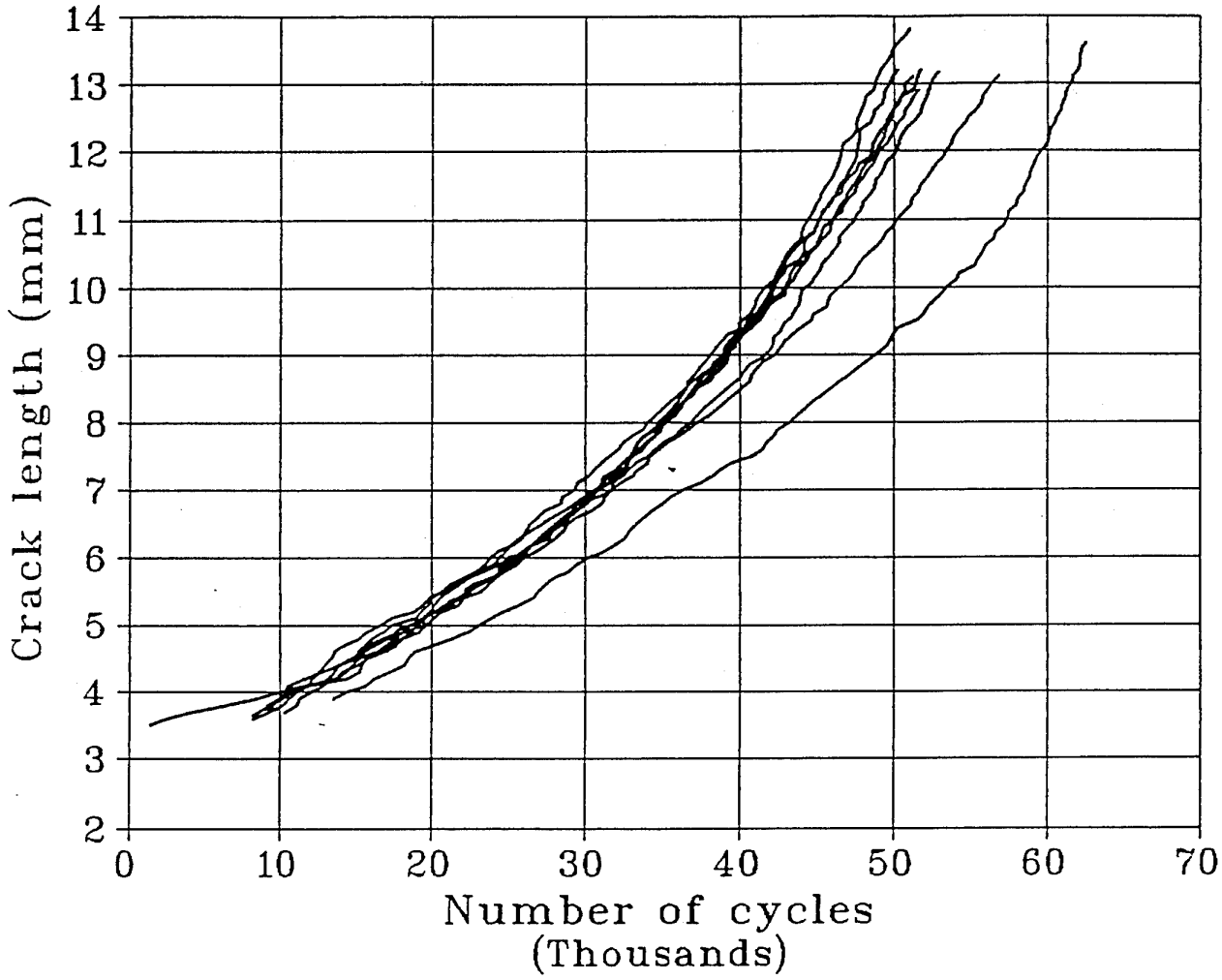

Fig. 28. Crack growth curves of the specimen No. 6 reduced via their regression curves to the common initial point (a_0=3mm, N_{0_i}=0).

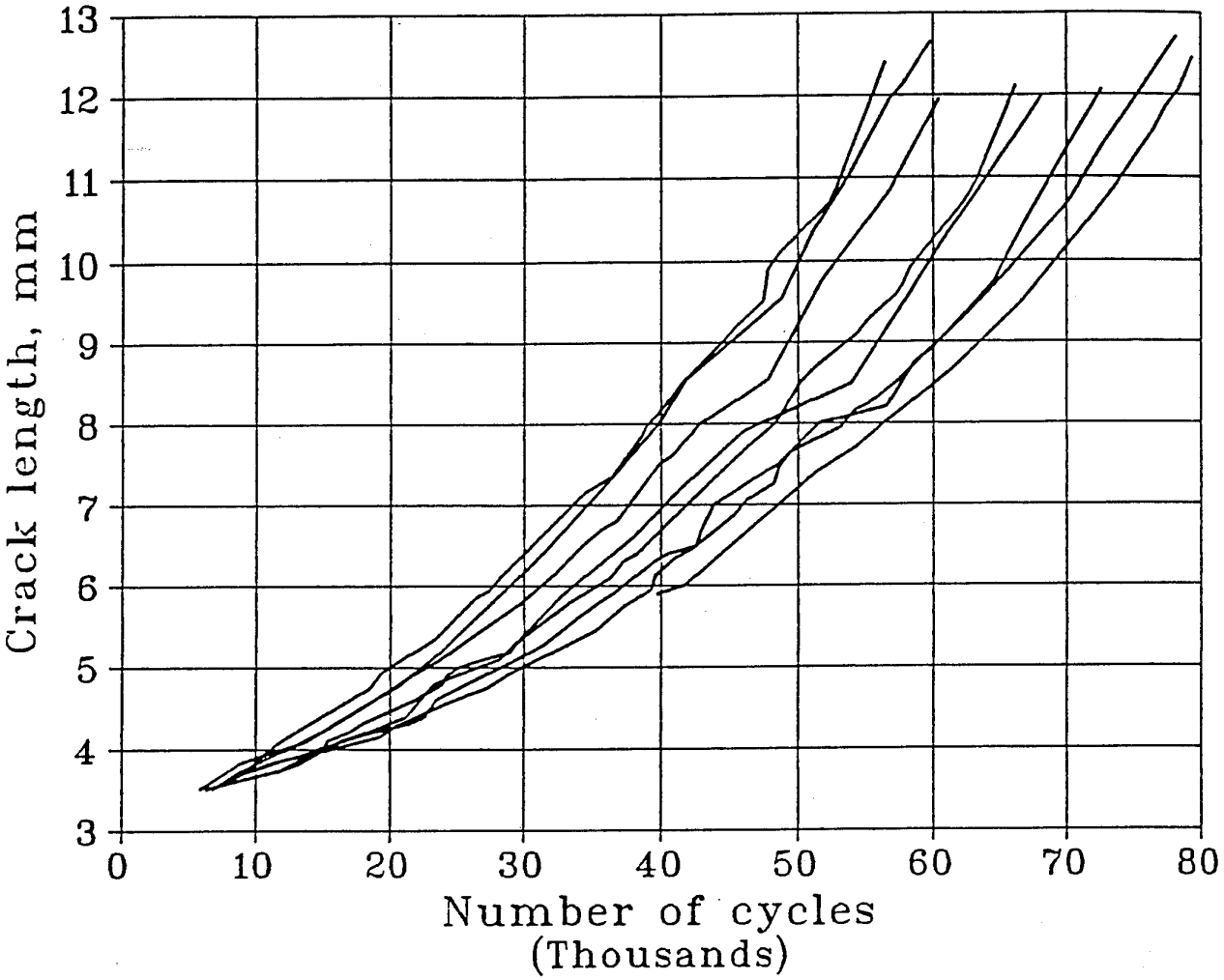

Fig. 29. Crack growth curves of the specimen No. 7 reduced via their regression curves to the common initial point (a_0=3mm, N_{0_i}=0).

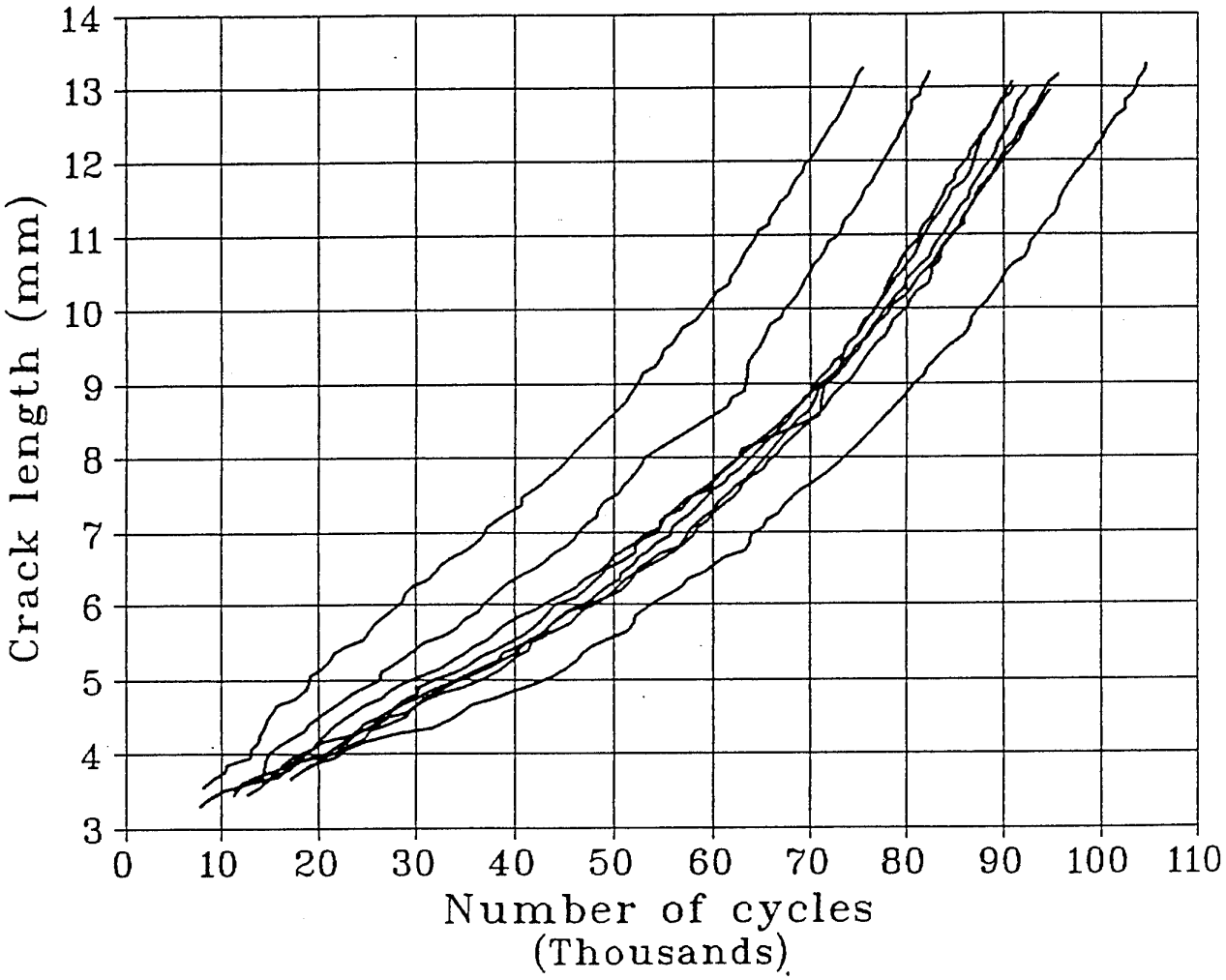

Fig. 30. Crack growth curves of the specimen No. 8 reduced via their regression curves to the common initial point (a_0=3mm, N_{0_i}=0).

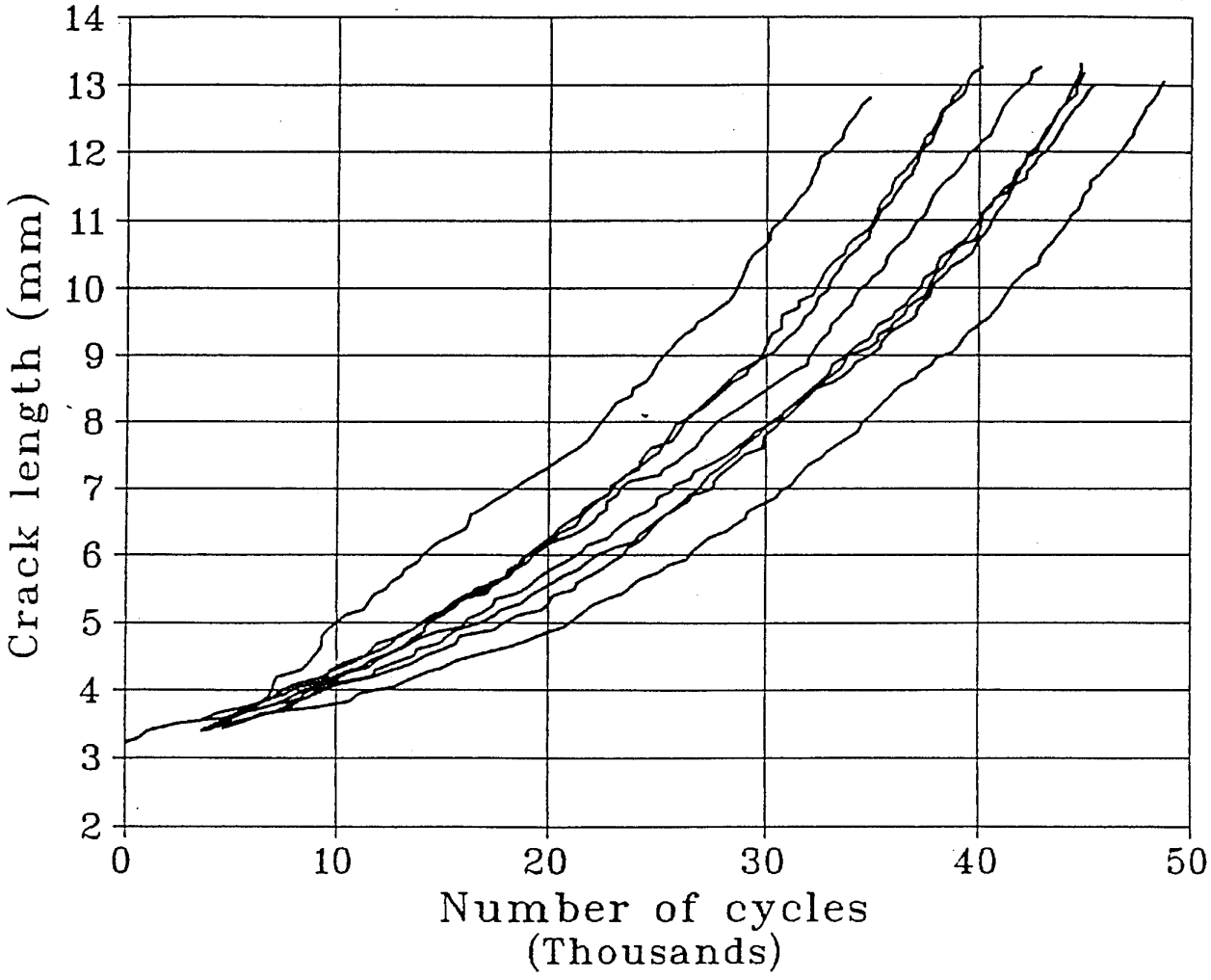

Fig. 31. Crack growth curves of the specimen No. 9 reduced via their regression curves to the common initial point (a_0=3mm, N_{0_i}=0).

The values of global exponent m determined in the case of the random loadings are confined by the range 2.1-2.16, which is somewhat lower than in the case of CA-loading, being 2.47-2.56.

4.4 Crack growth under random loading with superimposed overloads

For the study of the overload influence on the random loading crack growth the following parameters have been chosen for the base-line random loading process: P_{mean} = 24500NB, Std = 3920N and elimination threshold 2 Std. From time to time an overload peaks of the magnitude P_{OVL} = 64680N was superimposed on the base-line random loading. The magnitude of the overloads was about 1.5 times higher than the greatest load of the base-line random loading, P_{max}. The RL greatest load was estimated as follows:

$$P_{max} = P_{mean} + 4.25 \cdot Std.$$

where 4.25 corresponds to a highest division of the reversal transition matrix given in Table 1.

The time between the successive overloads was chosen to be greater than the temporary arrest time of all the cracks in the specimen. Fig. 32 exhibits crack growth curves of the multicrack specimen (specimen No. 10) tested under random loading with the superimposed overloads. Application of the overloads caused significant increase of the crack life time as compared with the specimen No. 8 tested under the same conditions except overloads.

Fig. 33 shows delay time data versus crack length. As can be seen from Fig. 33 increase of crack length from 3mm to 9mm caused threefold increase of the delay time. Further crack length increase up to 12.5 mm do not make for delay time increase, on the contrary, a tendency to decrease of delay time is observed.

As in the case of CA-loading, also under the RL-loading, the overloads cause enhanced local plastic deformation at the crack tip, changing the residual stress field near the crack tip.

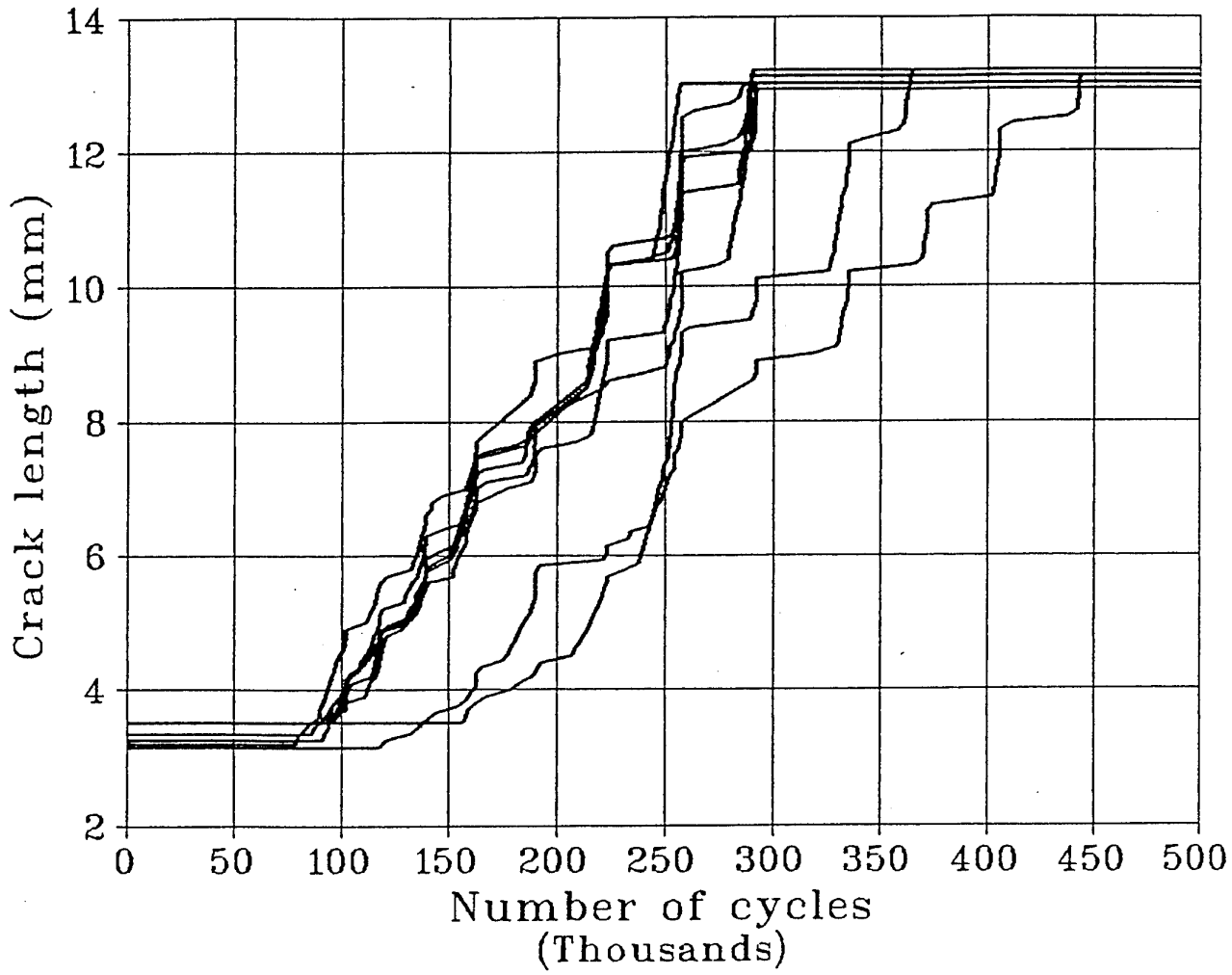

Fig. 32 Crack growth curves corresponding to the RL-loading with superimposed overloads (Specimen No. 10). Note horizontal segments of the curves corresponding to the after overload delay times.

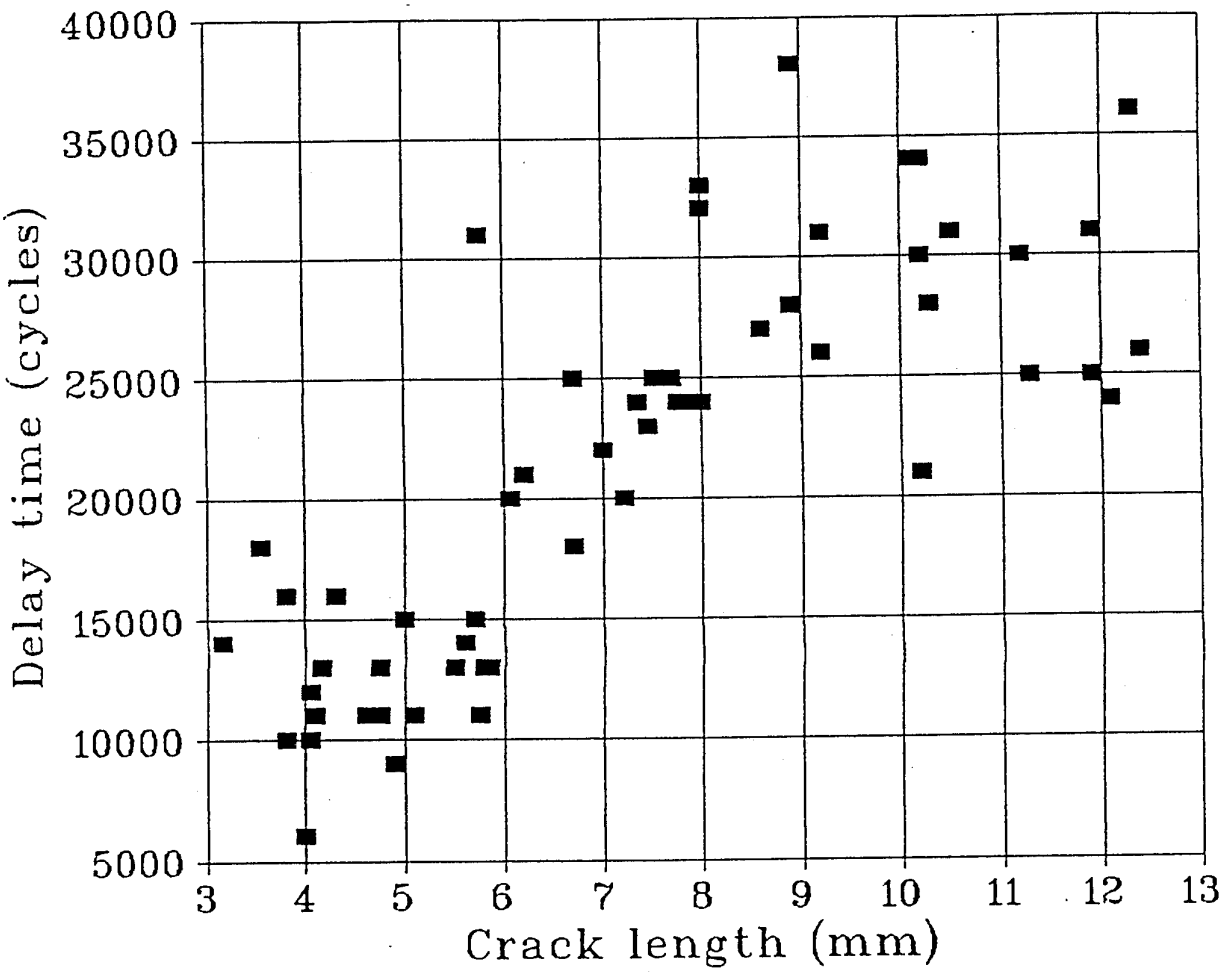

Fig. 33. Delay time as a function of the crack length.

In Fig. 34 one of the cracks grown in the specimen No. 10 is shown. It can be easily seen that at the crack arrest locations the double slanted deformation lines (moustaches) are created. It is also seen that the width of the deformation zone increases with increase of the crack length.

5. Discussion

The present work was devoted to experimental study of fatigue behaviour of arrays of simultaneously growing cracks under random loading histories deduced from a stationary Gaussian random processes. The future work will include the throughout analysis of the experimental results, development of a mathematical model describing fatigue crack growth as well as verification of the developed and existing in literature approaches. In the following a brief analysis of the random loading generation procedure as well as the test results is given.

The method used for generation of the random loading is based on creating a single loading history according to a given autocorrelation function. This history should be sufficiently long to represent all the stochastic characteristics of the random process which is supposed to be an ergodic Gaussian random process. For fatigue testing and analysis only succession of peaks and troughs is important, whereas the intermediate values of the random process are of minor importance if any. Therefore, the succession of the peaks and troughs of the generated loading history could be arranged in the time so to provide the most effective performance of the testing machine. For instance a constant loading rate may be specified [16]. An alternative mode of the constant time interval between the peaks and troughs was used in the performed tests. It allowed to solve effectively the problems of the test control and data acquisition.

The further "deformation" of the initially generated random loading history is caused by elimination of the small load ranges which, supposedly, does not

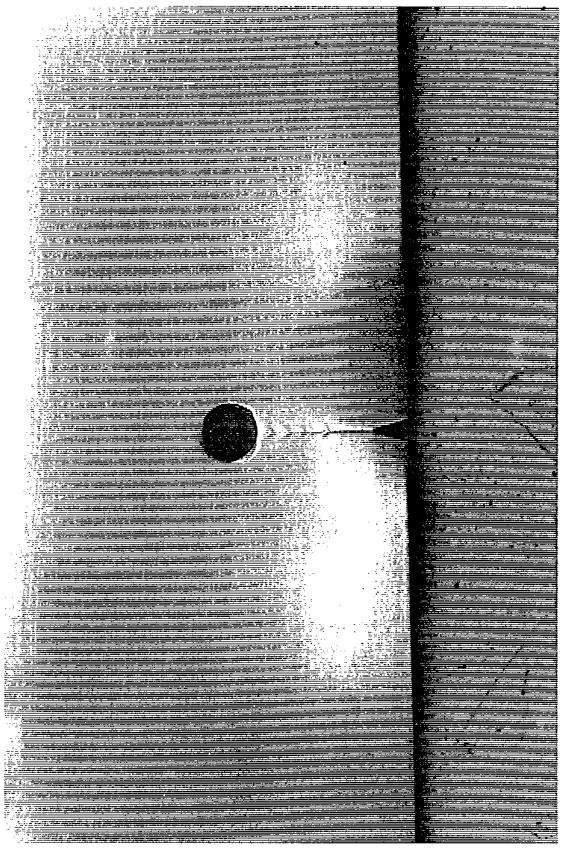

Fig. 34. Deformation lines generated by the overload peaks.

contribute to the crack growth. For the initial loading history used in the performed tests the elimination with the threshold equal to one standard deviation of the process cut 10 times the peak and trough number. Using as an elimination threshold the value of two standard deviations the peak and trough number was additionally cut in a half. Correspondingly the test time was reduced 10 and 20 times without distortion of the test results since the eliminated load ranges almost do not influence the crack growth.

After elimination of the small load ranges the average time interval between successive reversals became much longer than in the initial loading history. If this interval is greater than the maximum time interval of correlation between the values of the process (radius of correlation) the successive reversals could be considered as independent values. If radius of correlation is greater than one average inter-reversal interval but less than two such intervals so the succession of the reversals of the reduced loading history could be considered as a discrete process which could be determined by a Markov transition probability matrix. Two transition probability matrices were derived from the reduced loading histories: the first for the elimination threshold of one standard deviation, and the second for the threshold of two standard deviations. Analysis of the loading histories and the autocorrelation function (Fig. 9) shows that the above Markov property of the reversal succession certainly holds for the loading history reduced with the two standard deviations threshold. For the lower thresholds application of the Markov transition probability matrix approach should be checked by comparative rain-flow analyses of both the initial loading history and that generated by the Markov transition probability matrix.

The developed, in the course of the work, procedure for generation of the random loading history and its numerical rain-flow analysis could be applied also for verification of empirical formulae for rain-flow amplitude distribution [19, 20].

The tests under constant amplitude loading were performed as a reference to the

random loading tests. The interval of the stress intensity factor ΔK alteration from 5.3 MPa$\sqrt{m}$ to 11.1 MPa$\sqrt{m}$ corresponding to the crack growth from 3mm to 13mm is in the limits of application of the Paris power law of the fatigue crack growth. So the parameters of the Paris law determined as a result of the test for a number of the cracks will be used in the analysis of the stochastic properties of the material pertaining to the fatigue crack growth. The divergence of the crack curves which is well known from the tests of the specimens containing a single crack [21] was somewhat surprising in the test of the multicrack specimen since the loading of all the cracks is identical if one disregards the random nature of material medium. An adequate model of stochastic material field will be developed in continuation of the work in order to explain the divergence of the crack curves with their growth and enable reliable estimation of the crack growth life.

In the test under constant amplitude loading with superimposed overloads the temporary arrest of the crack growth was observed after application of the large overloads. The following concepts have been proposed to explain overloads influence:

a) effects associated with crack tip plastic zone formation and creation of local residual stress [10, 11, 22-24];

b) crack branching and kinking [25];

c) effects associated with crack closure [12-17].

Probabilistic approach recently proposed [26-31], incorporated load interaction in the random loading approach. Nevertheless the adequate explanation of the load interaction effects is still far from its completion. Further work is needed to achieve more complete description of the problem. The development of an adequate model of the fatigue crack behaviour is planned in order to achieve better explanation of the above effects.

Similar effects of the crack curves diversion and temporary crack arrest were found by the tests under random loading and random loading with superimposed

overloads correspondingly. As in the tests under constant amplitude loading the crack growth time scatter is about 30-40% irrespective of the crack length. From the two parameters of the random loading process, the standard deviation and the mean value, the first has stronger effect on the crack life time. Thus increase of 25% of the standard deviation causes crack life time reduction of about 20%, and 50% increase of the standard deviation decreases fatigue crack life time almost twice. On the other hand, 40% increase of the mean load reduces crack life time only by 25%.

Overloads superimposed on the random loading cause as in the constant amplitude loading a temporary crack arrest. The overloads applied were of the constant magnitude of 64680N corresponding to the stress intensity factor from 17.6 $MPa\sqrt{m}$ at 3mm crack length to 36.6 $MPa\sqrt{m}$ at 13mm crack length. The overloads caused in our cause up to 500% increase of the crack life time as compared with the analogous specimen tested without overloads. The delay time caused by overloads increases significantly (4 times) with the crack growth. The more severe retardation effect by the large scale loads is manifested not only after overloads but also by interaction of the loads in the base-line random loading. Lower values of the exponent m of the Paris law for the crack growth under random loading as compared with those pertaining to the constant amplitude loading indicate a growing influence of the large-scale loads with the crack growth.

6. Summary and Conclusions

The results obtained in the course of the present investigation can be summarised as follows:

1. A procedure for generation of the random loading histories according to the given autocorrelation function is developed.
2. The procedure includes elimination of the small amplitude cycles for the

purpose of the test acceleration.

3. The succession of the maxima and minima of the random loading history after elimination of small amplitude cycles can be considered as a discrete Markov process. An adequate transition probability matrix pertaining to this process was established from the generated loading history and used for real time generation of the random loading during the tests.
4. The statistical study of the fatigue crack growth in the aluminium alloy 7075-T6 multicrack specimens was performed. This study includes crack growth under constant amplitude and random loadings as well as CA and RL loadings with superimposed overloads.
5. A computerised system based on Instron testing machine was developed for test control and monitoring of crack growth using Kyowa crack propagation gauges.
6. The obtained totality of the crack growth curves was used for determination of the crack growth life time scatter.
7. The Paris crack growth law parameters were determined for both the constant amplitude and the random loadings. The curvature of the crack growth curves characterised by the exponent m is greater for the constant amplitude loading ($m \simeq 2.5$) than for the random loading ($m \simeq 2.1$).
8. The crack growth life time under random loading decreases with decrease of mean value and especially with decrease of standard deviation of the random process.
9. The overloads cause temporary arrest of the crack both in the constant amplitude and random loadings. The delay time caused by the overloads increases with overload ratio and with overall increase of the stress intensity factor level due to increase of the crack length.
10. Obtained results are the basis for development of a stochastic model describing crack growth under random loading.

Acknowledgement

The authors wish to acknowledge the United States Air Force (USAF) for funding this research program.

Special thanks to Lt. Col. Dr. A.M. Janiszewski, Structure and Materials of the European Office of Aerospace Resaerch and Development of the USAF, for assistance and support of this research.

Thanks also to Maj. Dr. D. J. Stech, Chief Structure and Materials of European Office of Aerospace Research and Development of the USAF, for his interest in this research.

REFERENCES

1. R. Arone, S. Ustilovsky, et al., A system for simultaneous monitoring of random crack arrays under random or/and constant amplitude loading. *The 29th Israel Conference on Mechanical Engineering*, pp. 5.3.3-1 - 5.3.3-8.
2. R. Arone, S. Ustilovsky et al., Simulation of random fatigue crack growth. *The 25th Israel Conference on Mechanical Engineering*, pp. 325-330.
3. ASTM E8-93. Test methods for tension testing of metallic materials.
4. SAE J454-91. General data on wrought aluminium alloys.
5. M. Bily, Dependability of mechanical systems. *Elsevier Amsterdam*, Oxford, New York, Tokyo, 1989.
6. ASTM E1049-85 (1990). Practice for cycle counting in fatigue analysis.
7. J. Schijve, Observations on the reduction of fatigue crack growth propagation under variable-amplitude loading. *Fatigue Crack Growth under Spectrum Loads, ASTM STP 595* (1976), pp. 3-25.
8. R.I. Stephens, D.K. Chen, and B.W. Hom, Fatigue crack growth with negative stress ratio following single overloads in 2024-T3 and 7056-T6 aluminum alloys, *ibid.*, pp. 27-37.
9. C. Bathias and M Vancorn, Mechanisms of overload effect on fatigue crack propagation in aluminium alloys. *Eng. Fract. Mech.*, 10, (1978), pp. 409-424.
10. S. Matsuoka and K. Tanaka. Delayed retardation phenomenon of fatigue crack growth resulting from a single application of overload. *Eng. Fract. Mech..*, 10, (1978), pp. 515-525.
11. T.D. Gray and J.P. Gallagher, Predicting fatigue crack retardation following a single overload using a modified Wheeler model. *Mechanics of Crack Growth ASTM STP 590* (1976), pp. 331-344.
12. W. Elber, The significance of fatigue crack closure. *Damage Tolerance in Aircraft Structures, ASTM STP 486* (1971), pp. 230-242.

13. A.U. de Koning, A simple crack closure model for prediction of fatigue crack growth rates under variable amplitude loading. *Fracture Mechanics: Thirteen Conference, ASTM STP 748* (1981), pp. 6-3-85.

14. J.C. Newman, A Crack-closure model for predicting fatigue crack growth under aircraft spectrum loading, *Methods and Models for Predicting Fatigue Crack Growth under Random Loading, ASTM STP 748* (1981), pp. 53-84.

15. J.C. Newman, Prediction of fatigue crack growth under variable-amplitude and spectrum loading using a closure model. *Design of Fatigue and Fracture Resistant Structures, ASTM STP 761* (1982), pp. 255-277.

16. H. Fuhring and T. Seeger, Dugdale crack closure analysis of fatigue cracks under constant amplitude loading. *Eng. Fract. Mech.*, 11, (1979), pp. 99-122.

17. H. Kobayashi and H. Nakamura. Investigation of fatigue crack closure analysis of plasticity induced crack closure. *Current Research on Fatigue Cracks.* Elsivier, Japan 1987, pp. 229-247.

18. J.K. Donald. Automated variable-amplitude fatigue crack growth technology, *Applications of Automation Technology to Fatigue and Fracture Testing*, ASTM STP 10982, A.A. Braun, N.E. Asbhaugh, and F.M. Smith, Eds., ASTM, Philadelphia, 1990, pp. 167-177.

19. I. Rychlik, Rain flow cycle distribution for a stationary Gaussian load process. *Stat. Res. Rep.* 1986: 4 (University of Lund, Sweden, 1986), pp. 1-36.

20. N.W.M. Bishop and F. Sharratt. Fatigue life prediction from power spectral density data. *Environmental Engineering*, Vol. 2, Nos. 1 and 2, March and June 1989.

21. Virkler, D.H., Hillberry, B.M., Goel, P.H. (1978). The statistical nature of fatigue crack propagation, AFFDD-TR-78-43.

22. J. Willenborg, R.M. Engle, and H.A. Wood, A crack growth retardation model using an effective stress concept. *AFFDL-TM0-FBR-81-1* (Air Force Dynamics Laboratory, Dayton, OH, USA, 1971).

23. O. Wheeler, Spectrum loading and crack growth. *J. Basic Eng.* 94D (1972), pp. 181-186.

24. W.S. Johnson, Multi-parameter yield zone model for predicting spectrum loading, *Methods and Models for Predicting Fatigue Crack Growth under Random Loading, ASTM STP 748* (1981), pp. 85-102.

25. S. Suresh, Micromechanism of fatigue crack growth retardation following overloads. *Eng. Fract. Mech.*, 18, (1983), pp. 577-599.

26. R. Arone, Fatigue crack growth under random overloads superimposed on constant amplitude cyclic loading. *Eng. Fract. Mech.*, 24 (1986), pp. 223-232.

27. R. Arone, On retardation effects during fatigue crack growth under random overloads. *Eng. Fract. Mech.*, 27 (1987), pp. 83-89.

28. R. Arone, Conservative estimation of crack growth under random overloads. *Eng. Fract. Mech.*, 127, (1987), pp. 83-89.

29. R. Arone, Influence of random overloads on fatigue crack life time and reliability. *Eng. Fract. Mech.*, 30, (1988), pp. 361-371.

30. R. Arone, Application of Wheeler retardation model for assessment of fatigue crack lifetime under random overloads. *Int. J. Fatigue,* 12 (1990), pp. 275-281.

31. R. Arone, "Application of closure concept to estimation of lifetime of fatigue crack propagating under random load," *J. Mechanical Behaviour of Materials,* vol. 3, 1991, pp. 192-156.